MASS AND STIFFNESS SPECTROMETRY OF NANOPARTICLES AND BIO-MOLECULES BY NANOELECTROMECHANICAL SYSTEMS

A THESIS SUBMITTED TO

THE GRADUATE SCHOOL OF ENGINEERING AND SCIENCE

OF BILKENT UNIVERSITY

IN PARTIAL FULFILLMENT OF THE REQUIREMENTS FOR

THE DEGREE OF

MASTER OF SCIENCE

IN

MECHANICAL ENGINEERING

By

Ezgi Orhan

August 2018

MASS AND STIFFNESS SPECTROMETRY OF NANOPARTICLES AND BIO-MOLECULES BY NANOELECTROMECHANICAL SYSTEMS
By Ezgi Orhan
August 2018

We certify that we have read this thesis and that in our opinion it is fully adequate, in scope and in quality, as a thesis for the degree of Master of Science.

Mehmet Selim Hanay(Advisor)

Onur Özcan

Burhanettin Erdem Alaca

Approved for the Graduate School of Engineering and Science:

Ezhan Karaşan
Director of the Graduate School

ABSTRACT

MASS AND STIFFNESS SPECTROMETRY OF NANOPARTICLES AND BIO-MOLECULES BY NANOELECTROMECHANICAL SYSTEMS

Ezgi Orhan
M.S. in Mechanical Engineering
Advisor: Mehmet Selim Hanay
August 2018

Mass spectrometry (MS) is a technique used frequently in mass measurements in order to identify mass of the molecules. Nanoelectromechanical systems are highly sensitive to adhered species, thus using NEMS devices, it is possible to perform NEMS-MS where not only the inertial mass of the molecules but also the position of the adhered particle can be found out by resolving the adsorbate-induced frequency shifts in the first two modes.By using frequency shifts obtained from three mechanical modes, it is possible to obtain stiffness of the adsorbate in addition to its mass and position on the resonator when the Youngs modulus of the analyte and the resonant structure are comparable. For soft analytes, multi-mode information can be used to obtain shape properties of analytes and allows for image reconstruction from global image features. In order to conduct our experiments, we fabricate NEMS resonators whose transduction method is electrothermal actuation and piezoresistive detection. Fabrications of the devices are completed in National Nanotechnology Research Center (UNAM) in Bilkent University and Sabancı University Nanotechnology Research and Application Center (SUNUM).Initially, low vacuum apparatus is built to perform NEMS-MS using Electrospray Ionization(ESI) for molecule delivery. In order to direct particles to resonator, the fabrication of a doubly clamped beam is planned in a way that the orifice was etched through silicon wafer from the backside with KOH etch.This fabrication method, however, is tedious and hard to fabricate consistently.Then, Matrix Assisted Laser Desorption and Ionization (MALDI) is implemented to deliver particles towards the resonator.Different analyte types which are gold nanoparticles, centrosome organelles of HeLa cells and M13ke bacteriophages are used in the experiments.We use first four out-of-plane modes of the doubly-clamped beam resonator for real-time study of the adsorbates. For biomolecule detection, care was taken to prevent uniform coverage of matrix molecules. Phase-locked-loop(PLL) operation is simultaneously performed for the first four modes of the resonator.Using frequency shifts of the four modes due to the adsorption, we propose a method in which we assume the analytes adhered on the beam are hemispherical to obtain mass and stifffness, size and positions of the analytes. Using three mechanical modes, stiffness, mass and position vaues are calculated.

Keywords: NEMS,Nanofabrication, Electrothermal Actuation, Piezoresistive Detection, Multimode Mass Sensing, Mass Spectrometry, Stiffness Spectrometry, Electrospray Ionization, Matrix Assisted Laser Desorption and Ionization.

ÖZET

NANOPARÇACIK VE BİO-MOLEKÜLLERİN KÜTLE VE SERTLİKLERİNİN NANOELEKTROMEKANİK SİSTEMLER İLE ÖLÇÜLMESİ

Ezgi Orhan
Makine Mühendisliği, Yüksek Lisans
Tez Danışmanı: Mehmet Selim Hanay
Ağustos 2018

Kütle Spektrometrisi moleküllerin kütlesinin ölçülmesinde sıklıkla kullanılan bir tekniktir. Nanoelektromekanik Sistemler kullanlarak sensör üzerine gelen parçacğın kütlesini ve mekanik yapı üzerindeki konumunu bulmak, yapının ilk iki titreşim mod frekaısındaki değişimlere bakılarak mümkündür. Ayrıca üç mod titreşim modundaki frekans kaymaları ile de Esneklik Katsayısı, kütle ve mekanik yapı üzerindeki pozisyon bilgilerine ulaşmak mümkündür. Daha fazla mekanik moddan alınan frekans değişimi bilgileri yumuşak analitlerin şekil özelliklerine ulaşmak için kullanlabilir ve global şekil bilgisinin oluşturulmasına izin verir. Deneyleri gerçekleştirmek için kullanılan cihazların üretim aşamaları Bilkent Üniversitesi'ndeki Uluslararası Nanoteknoloji Merkezi'nde ve Sabanı Üniversitesi Nanoteknoloji Araştrma ve Uygulama Merkezi'nde tamamlanmıştır. İlk olarak Elektrospray Iyonizasyon yöntemi ile moleküllerin oluşturulması ve NEMS'e iletilmesi için düşük vakumda kullanlacak deney düzeneği kurulmuştur. Silikon devre levhasının arkadan KOH ile aşındırılması ile çift ankastreli yapı üretilmiştir ancak bu yöntemle üretim tekrar edilmesi zor ve zahmetlidir. Daha sonra, analiti NEMS yüzeyine göndermek için Matriks Destekli Lazer Yüzeyden Çılarma ve İyonizasyon (MALDI) yöntemi altın nanoparçacıkları ,HeLa hücrelerinden alınan sentrozom organeli ve M13ke bakteriyofaj deneylerinde kullanılmıştır.Çift ankastreli yapının ilk dört düzlem dışı modu gerçek zamanlı deneylerde kullanılmıştır. Biyomolekül deneylerinde matrix tuzunun yapının tüm yüzeyinin kaplanmamasına çalışılmıştır. Faza kilitli Çevrim yöntemi her mod içın eş zamanlı olarak uygulanmıştır. Yüzeye tutunan analitin yarattığı frekans kaymalarını kullanarak, kütle, büyüklük, Esneklik Katsayısı ve pozisyon ölçümü için analitin yarıküre olduğu varsayılarak bir yöntem önerilmiştir ve üç mod frekans kaymaları kullanılarak kütle, Esneklik Katsayısı ve pozisyon değerleri bulunmuştur.

Anahtar sözcükler: NEMS, Nanofabrikasyon, Elektrotermal Sürme, Piezorezistif Okuma,Çok Modlu Kütle Ölçümü, Kütle Spektrometrisi, Sertlik Spektrometrisi, Elektrosprey İyonizasyonu, Matriks Destekli Lazer Yüzeyden Çıkarma ve İyonizasyonu .

Acknowledgement

First, I would like to enounce how grateful I am to be one of the graduate students of Prof. Selim Hanay. His continuous guidance and support to overcome problems and challenges I encountered with during my research motivated me a lot. I believe that I am going to take him as a role model throughout my life regarding his hardworking, diligent and idealistic stance.

I also want to thank my thesis comittee, Prof. Erdem Alaca and Prof. Onur Özcan for their time in both my thesis defense and recommendation letters in my Ph.D. applications. I want to thank my friends Hande Aydoğmuş, Mehmet Kelleci, Selçuk Oğuz Erbil and Levent Aslanbaş.We spent not only graduate school years but also undergraduate years together. I feel so lucky to know and share these memorable times with you.Thank you Mert Yüksel for your friendship and support in fabrication for NEMS devices and MALDI experiments and also I should thank him and Mustafa Kara for our discussion and their contributions on the theory. I would like to thank Atakan Bekir Arı and Mustafa Çağatay Karakan for their guidance in microfabrication and measurements in the first two years of this study. I feel happy since I will have a chance of working with you in my Ph.D. study. I want to thank Utku Hatipoğlu and Arda Seçme for their contributions. Administrative assistant of our depatment, Ela Baycan and administrative assistant of Hanay Group, Güliz Erdal, thank you for your help and support.

I greatly enjoyed the chance to spend graduate school with wonderful people in Bilkent University. Dilara Uslu, thank you for your support and friendship in making good times better and hard times easier. Umutcan Çalışkan, Cem Kurt, Cem Aygül thank you for making hard times of writing my thesis enjoyable. Rico Morasata, Ozan Temiz, Müge Özcan, İbrahim Nasuh Yıldıran, thank you for your friendship and discussion we had in lectures.

I should also thank Dr. Cenk Yanık for his collaboration in microfabrication, Ezgi Odabaşı for preparing centrosome test tubes and Recep Erdem Ahan for his

help in buffer exchange process, Elif Özçelik for preparing bacteriophages.

I will be always grateful to my parents Sevgi and Gökhan, who supported me in every step of my life and directed me to correct ways when I felt lost. My twin sister Gizem, thank you for being with me from the beginning of my life and it is so good to know you will be there whenever I need.

Contents

List of Figures

List of Tables

Chapter 1

Introduction

1.1 Nanoelectromechanical Systems(NEMS)

With the improvements in microfabrication techniques that selectively etch the materials and add new structural layers, microelectromechanical Systems (MEMS) research and development resulted in variety of devices including micro-valves, micro-pumps, micro-resonators. Further developments in fabrication techniques revealed nanometer scale devices. Nanoelectromechanical systems(NEMS) offer high sensitivity to external perturbations such as mass and they are manufactured relatively cheaply in chip scale with the semiconductor technology developed for Integrated Circuits. Nanoelectromechanical systems(NEMS) are continuous mechanical structures and actuation and detection of their motion occurs via transduction between electrical and mechanical signals. NEMS are next miniaturization step of microelectromechanical systems thus at least one dimension of these structures are less than a micrometer. Offering microwave resonance frequencies [1], high quality factors in the level of tens of thousands [2] has resulted in improvements in biological studies [3], gas sensing application[4, 5] and mass sensing [6–20].

In this study we use doubly clamped beams in their resonant motion. Their motion is just like a harmonic oscillator and it creates kinetic energy on the beam and due to their dynamic response, potential energy arises. The equation below shows harmonic oscillator model for NEMS response.

$$\ddot{x}(t) + \frac{\omega_0}{Q}\dot{x}(t) + {\omega_0}^2 x(t) = \frac{f(t)}{m_{\ eff}} \tag{1.1}$$

Their resonance frequencies can be found by equating potential and kinetic energy of the device. When a particle adheres to the beam, effective mass of the device increases and this extra mass causes abrupt change in resonance frequency. By measuring the NEMS resonance frequency continuously, NEMS device is used to deduce physical properties such as mass, stiffness, size of the particle landed on the beam.

1.2 Conventional Mass Spectrometry

Mass Spectrometry is a method that aims to measure the molecular weight of particles. It is based on generating analyte ions in gas-phase, separating those ions according to mass to charge ratio with the help of electromagnetic field and finally those molecules are directed to charge detector to count the ions. Since molecules produce multiple peaks,it is necessary that the system is capable of distinguishing different charge states in order to obtain mass value.

The most popular ionization techniques are Electro-spray Ionization (ESI) and Matrix Assisted Laser Desorption/Ionization(MALDI).Laureates John B. Fenn, Koichi Tanaka shared the Nobel Prize in Chemistry for 2002 for their works on two very important methods of chemical analysis applied to biological macromolecules.[21, 22]. Those techniques enabled the analysis of highly large molecules such as bio-macromolecules.

Mass analysis can be conducted with variety of ways which are Quadrupole Mass Analyzer, Ion- Trap Mass Analyzer, Time-of-Flight Mass Analyzer, Fourier Transform Ion Cyclotron Resonance Mass Spectrometer and Orbitrap Mass Analyzer [23]. The obtained data allow quantitative analysis and molecular mass of the analytes can be determined [24]. However,conventional mass spectrometry can not provide single-molecule measurements in general for analytes whose mass are above 100 kDa. This thesis includes the ionization part of the conventional MS and principles of ESI and MALDI methods will be explained.

1.2.1 Electrospray Ionization Method(ESI)

Electrospray was developed long before its use in mass spectrometry and it has become hotly preffered method for biomolecule analysis after its introduction to the field [25]. The theory related with mechanism of creating charged droplets was put forward by the researchers in the aerosol science. The method consist of three stages which are production of charged droplets at the capillary tip, droplet evaporation resulting in shrinkage in size and production of gas phase ions from highly charged droplets in atmospheric conditions[23].

As shown in the illustration below, high voltage (kV) is applied to the capillary tip having 1 mm outer diameter. Since the capillary tip is very thin, very high electric field occurs at the capillary tip. After generation of charged ES droplets, droplets undergo many cycles of evaporation and gas phase ions are produced. The cone shape formed is called Taylor cone and a fine jet appears at the cone tip.

The electric field at the capillary tip can be calculated with the relationship given as follows:

$$E_c = 2V_c/[r_c ln(4d/r_c)] \tag{1.2}$$

where V_c is applied potential to the capillary tip, r_c is outer radius of the capillary tip, d is the distance between tip and the counter electrode. When high voltage is turned on, E_c will cause a polarization and positive and negative electrolyte ions start to move. While positive ions accumulate near the surface of the meniscus, negative ions accumulate away from it. After that cone shape which can be seen in the figure above appears.

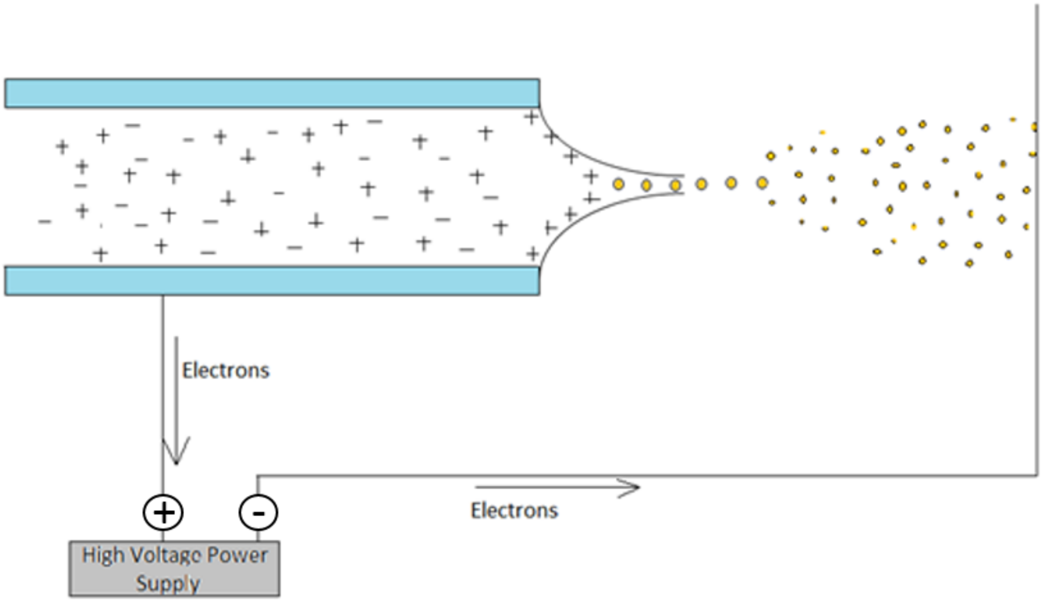

Figure 1.1: Illustration of ESI Process Occurring in Atmospheric Pressure Recreated From [23]. Creation of cone and a jet splits into positively charged droplets. Evaporation of droplets lead to production of gas phase ions

1.2.2 Matrix Assisted Laser Desorption and Ionization (MALDI)

MALDI is one of the two major modern ionization techniques. This method is a complex method due to the interactions of chemical and physical components and it leads to empirical work in the process of determining suitable matrices for analytes. The success with MALDI is dependent on finding correct matrix. After mixing analyte solution with matrix solution, the mixture is deposited on the target plate. When the target is bombarded with the laser source, desorption occurs. However, laser desorption does not mean that a molecule will be ionized it is a separate process from desorption.

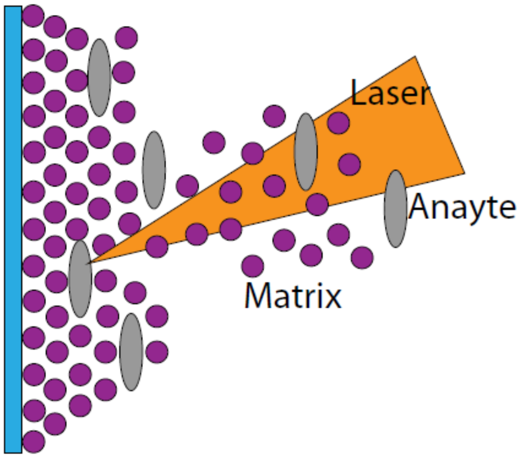

Figure 1.2: Illustration of MALDI process

When laser pulse hits the plate, matrix absorbs the laser light and it is desorbed with a several hundred meters per second velocity and propels the analyte at the same time. Typically, organic molecules have ionization potentials higher than 10 eV and most of the lasers have photon energies less than 6 eV, meaning that in order for ionization to occur, the molecule must absorb many photons. The nitrogen laser used in the experiments has 337 nm wavelength and 3.6 eV single photon energy [23].

1.3 Role of NEMS in Mass, Stiffness and Size Spectrometry

Mass sensing is one of the important application realms offered by NEMS technology due to their high quality factor and minuscule masses thus, high sensitivity to external perturbations. With conventional mass spectrometry, it is hard to detect larger ions due to its incapability of transporting large ions to the detector. However, NEMS-MS provides measurements of mega-dalton range particles as well. Mass resolution of the NEMS-MS depends on the device itself and it does not rely on mass to charge ratio. Thus it is possible to sense the particles in broad range. Additionally, NEMS-MS does not necessitate ionization of the particles and the comparison of NEMS-MS and TOF-MS has shown that neutral particle detection has been achieved successfully with NEMS-MS while TOF-MS is unable to detect those neutral particles [6].

The article published in 1995[7] have shown that the adsorption of molecules on cantilever can produce bending and thus cause resonance frequency shifts. Based on the shifts occurring in resonant frequencies of the NEMS devices, mass measurement experiments have been conducted for variety of biological and chemical sensing applications. The achievements presented in the last decade enabled femtogram [8], attogram [9] and finally zeptogram[2] level mass resolution. In 2005, the effect of mass position on mass responsivity have been investigated using a cantilever mass sensor. In this study, position of mass has been changed in small steps along the cantilever and the effect of this in the resonant frequency for several bending modes has been shown [10].

Analytical expression to determine mass and position of the attached particle on a cantilever has been derived and the finding was experimentally verified in 2007 [11]. Later, resonance frequency shifts obtained from airborne particles accreted on the microscale resonator was used to calculate mass of the particles [12].

While developments in mass sensing with the devices fabricated with top-down methods continue, devices produced by bottom-up methods such as Carbon nanotubes have shown ultrasensitive mass sensing [13, 14] and yoctogram resolution in mass sensing has been achieved [15].

For the first time, an approach towards real time mass spectrometry for single molecules has been shown in 2009 [16]. First and second resonance frequencies have been tracked simultaneously with Phase-Locked-loop (PLL) and frequency shifts obtained in real time used to verify the two-mode theory experimentally for single protein molecules in 2012 [17].

While two-mode theory offers mass and position information of the analyted landed on the beam, multimode resonance frequency shifts can be used to obtain information about stiffness of the particle as well. It was proposed that stiffness effect can be comparible and even higher than mass effect and can create positive frequency shifts[26] .More detailed theoretical analysis has been presented to calculate resonance frequency shift caused by stiffness of adhered viral nanotube and the effects of its orientation angle on strain enegry of the analyte were explained in 2014 [18]. By tracking the three resonant frequencies and solving the inverse problem, stiffness of the analytes also has been obtained in addition to mass, position [19]. A new methodology to obtain inertial image of a soft analyte using the multimodal frequency shifts caused by molecular adsorption events has been shown. The theory is verified by FEM simulations and experimental data [20].

1.4 Outline of Work

Chapter 1 stands for an introductory chapter explaining Nanoelectromechanical Systems(NEMS) and conventional mass spectrometry. Ionization methods, Electrospray Ionization(ESI) and Matrix Assisted Laser Desorption and Ionization(MALDI) that are also applicable for NEMS-MS and recent developments in the realm of mass, stiffness and size spectrometry are presented.

In Chapter 2, microfabrications steps are explained in detail, starting from the first E-beam Lithography process to wirebonding of a printed circuit board. Icp Dry Etch recipe that was developed in our lab previously is included as a table. After that, electromechanical transduction of NEMS devices are explained. Thermoelastic actuation and piezoresistive down-mixing methods are explained. Effects of LNA Gain and Bias Delta Frequency on the signal to background and signal to noise ratio are presented. DBOX, the measurement device used in the experiments conducted in this study is presented and a brief information related with Phase Locked Loop(PLL) is given. Allan Deviation and its effect on mass resolution are explained.

In chapter 3, ESI experimental set-up,and its preliminary experiments are presented. NEMS fabrication steps with KOH backetch are explained and problems encountered with ESI and device fabrication are stated.

In Chapter 4, construction of experimental set-up for NEMS-MALDI-MS is presented. Real time single molecule measurements are conducted for different types of analytes like gold nanoparticles, centrosome organelles and M13ke bacteriophages. NEMS resoantors are driven in four out of plane vibration modes at the same time and multimode information is used for mass, stiffness and size spectrometry. Frequency shifts of first two modes are used for mass and positions of the analytes. Since the stiffness effect is not included, the mass values give an approximate value. In order to reach more approximate result, stiffness of the analytes are also taken into consideration. Assuming that analytes adhered to the beam are hemispherical, we present theoretical calculations and equations for frequency shifts are given in an useful form.

The last chapter includes a summary of this M.S.thesis and provides a discussion related with the experiments in addition to future prospect.

Chapter 2

Fabrication and Transduction of NEMS resonators

2.1 Fabrication of NEMS resonators

Fabrication of the NEMS resonators starts with double side low stress, LPCVD grown silicon nitride wafers. This wafer ,100 nm Silicon nitride layer on top of 500 μm silicon substrate was purchased from University Wafer.

Although some of the resonators used in this work were fabricated in National Nanotechnology Research Center (UNAM), due to better alignment and resolution capabilities, Electron Beam Lithography steps of most of the resonators were conducted in Sabanci University Nanotechnology Research and Application Center (SUNUM).

1)100 nm thick low stress silicon nitride wafer grown on 500 m Silicon substrate is diced out of wafer as 10 mm x 10 mm

2)Bilayer PMMA 495 A4 and PMMA 950 A2 are spin coated on top of Silicon nitride with a thickness of 300 nm

3)Contact pads are defined with E-beam Lithography and after development PMMA layer dissolves as in the figure

4)4 nm Cr as an adhesion layer and 100 nm thick Au layer are deposited by thermal evaporation

■ Silicon 🟦 Silicon Nitride 🟨 Gold ▨ PMMA

5) After overnight Lift-off process gold contact pads appeared

6)Bilayer 300 nm PMMA coating for the next E-beam lithography step

7) Second E-beam Lithography step is applied in order to define gold electrodes which requires dose factor test for better accuracy beforehand

8) Second Cr and Au deposition by thermal evaporator. Thickness of the gold layer can be chosen such that resistance of the electrodes are around 50Ω

⬛ Silicon 🟦 Silicon Nitride 🟨 Gold 🟥 PMMA

9) Second lift-off process and gold electrodes are appeared

10) Third PMMA coating for the last E-beam lithography

11)Third E-beam lithography process in order to define borders of the doubly clamped beam. This step is critical and alignment of this layer should be done in such a way that electrodes are located in the center.

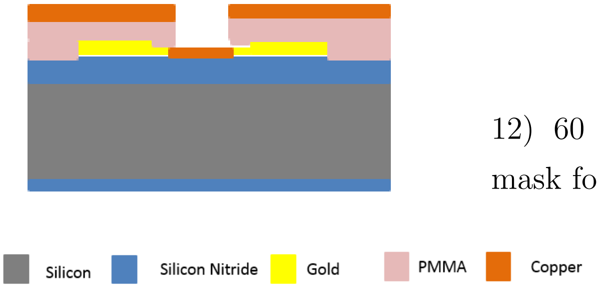

12) 60 nm Cu deposition as an etch mask for ICP processes

13)After Lift-off process and borders of the beam appeared.Before etch steps, conditioning procedure should be applied, which is running the recipe without etch sample to clean and condition inside of the chamber.

14) Anisotropic Silicon nitride etch in Inductively Coupled Plasma (ICP). Recipe used in this etch step is composed of CF_4 and CHF_3 gases

15)Isotropic Silicon etch in ICP in order to suspend resonator. Recipe used in this step is composed of SF_6 and CHF_3 gases

16) Wet etch to remove Cu layer. Aluminium Etchant is used for this step.

Etch recipe of Anisotropic Si_3N_4 and Isotropic Si etch are given in the table below. This recipe was developed by previous members of our group and used as it is for the fabrication of the resonators. and is applied for all Si_3N_4 resonators used in this work.

Table 2.1: Dry Etch Recipe

Dry Etch Recipe	Si_3N_4 Etch	Si Etch
Etchant Flow	20 sscm CF_4	15 sscm SF_6
Passivation Flow	3 sscm CHF_3	2 sscm CHF_3
Coil Power	400 Watt	150 Watt
Platen Power	100 Watt	30 Watt
Pressure	5 mTorr	10mTorr
Temperature	25 °C	25 °C
Time	1 min	4 min

It is better to apply these two etch steps simultaneously but if we can not do it for some reason, we can remove organic residues by applying oxygen plasma before etch steps. After completing etch processes, Scanning Electron Microscopy (SEM) should be used to check suspension of the beam. If there is no problem, etch mask can be removed by Aluminium etchant which is applicable to remove Cu layer as well.15 min was enough to remove 60 nm thick Cu layer. After checking at optical microscopy, one can put the sample into wet etchant for a few minutes until it is completely removed. When characterization of the NEMS resonator is completed, it is ready for wirebonding which is basically done by connecting contact pads to large copper layers on the printed circuit board (PCB) with thin wires. Here the purpose is to carry the electrical connections to larger area in order to drive the resonator and detect its response from SMA connectors.In this thesis, wirebonding of most samples was operated in METU-MEMS due to easier and quicker applicability of the wirebonder. Since it has ultrasonic sensors it can measure the distance between the tip and contact pad very accurately and it creates wedge-wedge bonding between contact pads and copper layers of PCB thus this reduces the time spent on wirebonding.

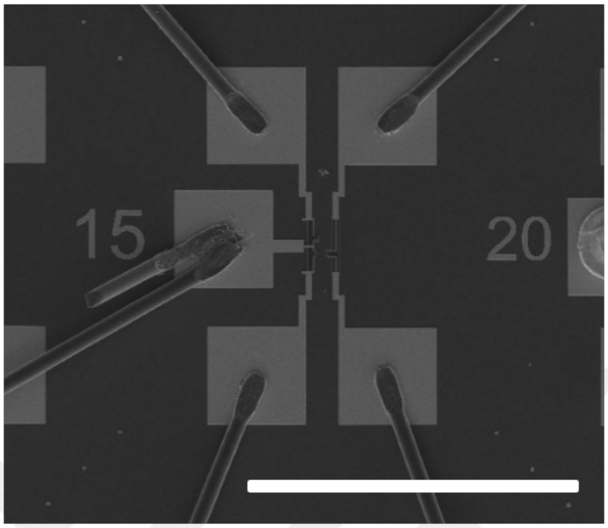

Figure 2.1: SEM image of wirebonded device. Scale bar is 500μm

2.2 Electromechanical Transduction

Transduction in general means conversion of a signal from one domain to another domain and transduction consists of two elements which are actuation and detection. Electromechanical transduction method relies on converting an electrical input to mechanical stimulus and output transducer convert mechanical response on the resonator back into electrical signal. [27].

There are lots of actuation and detection methods for NEMS transduction. NEMS resonators used in experiments utilize thermoelastic actuation and piezoresistive detection.

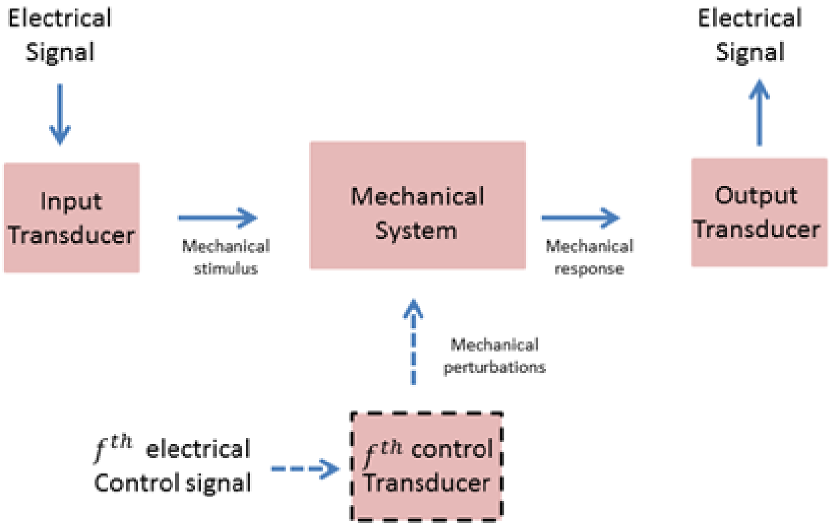

Figure 2.2: Representation of electromechanical device. Recreated from [27]

2.2.1 Thermoelastic Actuation

Thermoelastic actuation benefits from the fact that two materials have different thermal expansion coefficients. When a voltage is applied to the gold electrode located on Si_3N_4 beam, non-uniform expansion resulted from local heating creates thermal stress. Periodical change in tempeture at the resonance frequanecy of one of the vibration modes of the beam, amplitude of vibration will increase greatly [28].This actuation method is totally electronic and provides easy implementation however, it is hard to fabricate thin devices in width due to the existence of U-shape electrode on the beam. Thermoelastic actuation can be employed in two ways. First one is to apply only AC voltage to the drive electrode. Since the thermal power is proportional to the square of the voltage, resonance occurs when $w_d = w_m/2$. Second one is to apply DC+AC voltage to the drive electrode. This time system reaches resonance condition when $w_d = w_m$[29].

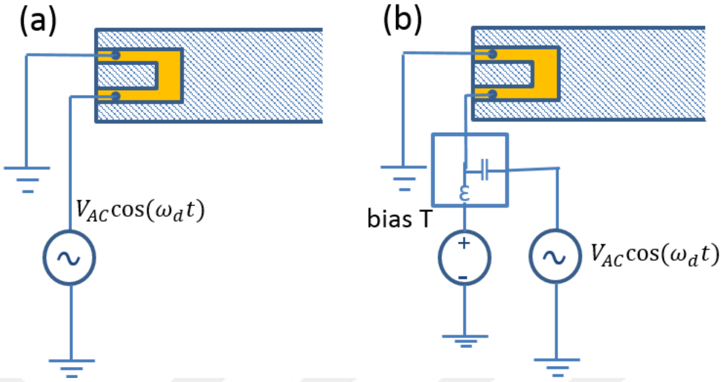

Figure 2.3: a)Thermoelastic actuation Schema AC voltage b) AC+DC voltage.Recreated from [29]

2.2.2 Piezoresistive Detection

This detection method utilizes piezoresistivity of the materials defined as change in resistance under the effect of strain [30]. There is no additional equipment necessary as in the optical and magnetomotive detection. The relation between strain and change in resistance is :

$$\frac{\Delta R}{R} = G\varepsilon(t) \tag{2.1}$$

In our resonators, change in resistance results from geometric effect [29] which is, change in the shape of gold electrode.During vibration, resistance of the gold electrode differs and the response of the beam can be read in Lock-In-Amplifiers. At moderately high frequencies, parasitic capacitances form a low pass filter having a cut-off frequency of $(\pi RC)^{-1}$ therefore high frequency terms are attenuated by this effect and at high frequencies, cable resonances also complicates the measurement. In order to read the response,downmixing schema can be implemented.To do that, a bias voltage having $\Delta\omega$ offset from the mechanical actuation frequency is applied to the detection electrode. Output voltage includes $cos(\Delta\omega t)$ and $cos(2\omega_d + \Delta\omega)t$ terms. Output signal passes through LPF and resultant signal having frequency is amplified before going to Lock-in-amplifier

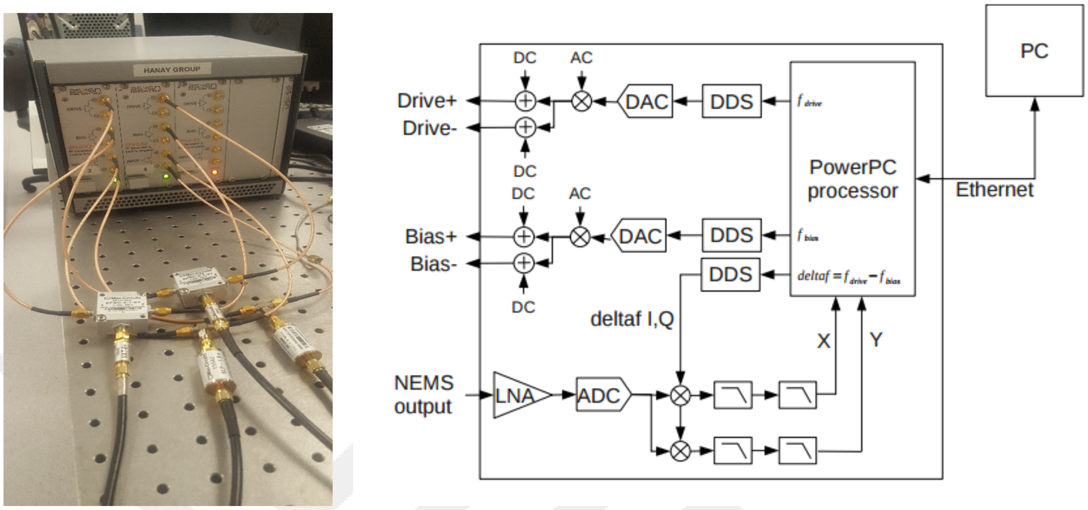

Figure 2.4: DBOX and Channel Architecture

input [31]. To read that signal, Lock-in-amplifier reference needs to have the same frequency with the input. In order to produce that signal, mixer takes two input of $V_{bias}(t) = Vcos(\omega + \Delta\omega)t$ and $Vcos(\omega t)$.

2.3 Measurement Setup

The measurements of this thesis were held in a commercial electronic instrument Dbox. It is special equipment for down-mixing and since it includes function generators and digital lock-in-amplifier(LIA), low noise amplifier(LNA) in it, no additional component is necessary. It is possible to generate AC and DC signals with this device and there is wide frequency range for Drive AC signal. It is very compact equipment and offers easy implementation.

DBOX offers open loop frequency sweep and closed loop operation and has a number of channels that can be operated at the same time and one channel can be operated in dual tone as well, which means it is possible to drive the NEMS resonator in its different mechanical modes simultaneously. In order to obtain better response, different parameters for LNA gain and bias delta frequency should be tried. Finding correct parameters can increase signal to background ratio and

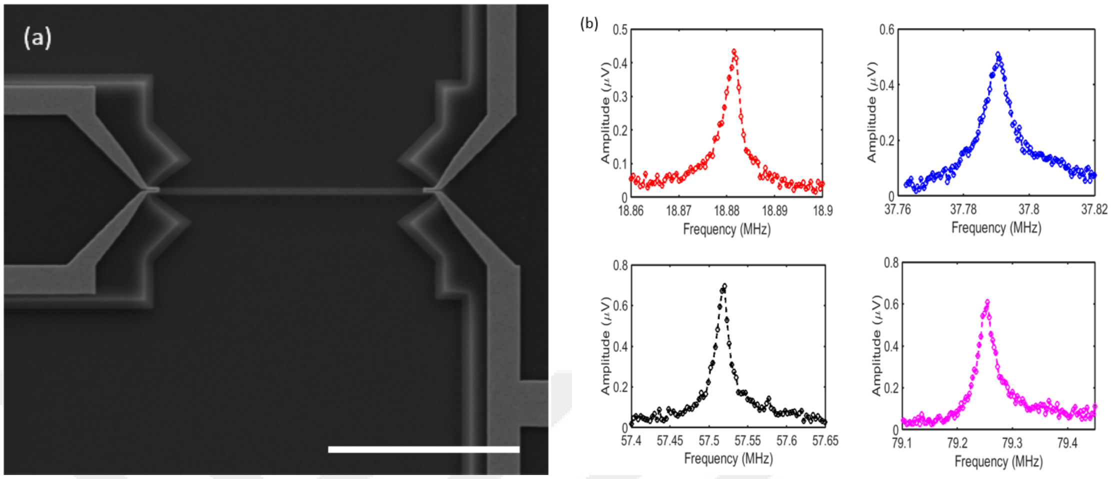

Figure 2.5: a) SEM image of NEMS resonator($15\mu m \times 370nm \times 100nm$) b) 1^{st}, 2^{nd}, 3^{rd} and 4^{th} Out of Plane Modes of NEMS resonator. Scale bar is $10\mu m$ for a)

signal to noise ratio of the NEMS response.

In this thesis, two DBOX channels was used in order to drive NEMS resonator in its four out of plane vibration modes. Since dual tone operation offered a chance of driving two modes simultaneously, two channels were sufficient for our purpose.After taking frequency sweep, it is possible to locate resonant modes and drive NEMS resonator in resonance frequency and any accreted particles on the resonator could be detected.

NEMS resonator is driven in its mechanical modes and the device is kept in resonance frequency all the time with a closed loop control called Phase-locked-loop (PLL). PLL is a feedback loop that includes voltage controlled oscillator to be locked into input signal coming from NEMS resonator and also it has a phase detector which compares the phase difference between input signal and NEMS response. Phase error signal then is sent to Loop filter (LP). LP is a simple RC filter and it removes unwanted high frequency components that may goes through PD. Hence frequency shifts that result from particle adsorption can be tracked and this allow us to store $\delta f/f$ for each driven modes. The figure below shows how PLL responds to a stimuli applied on frequency and PLL response time for each mode can be checked on.

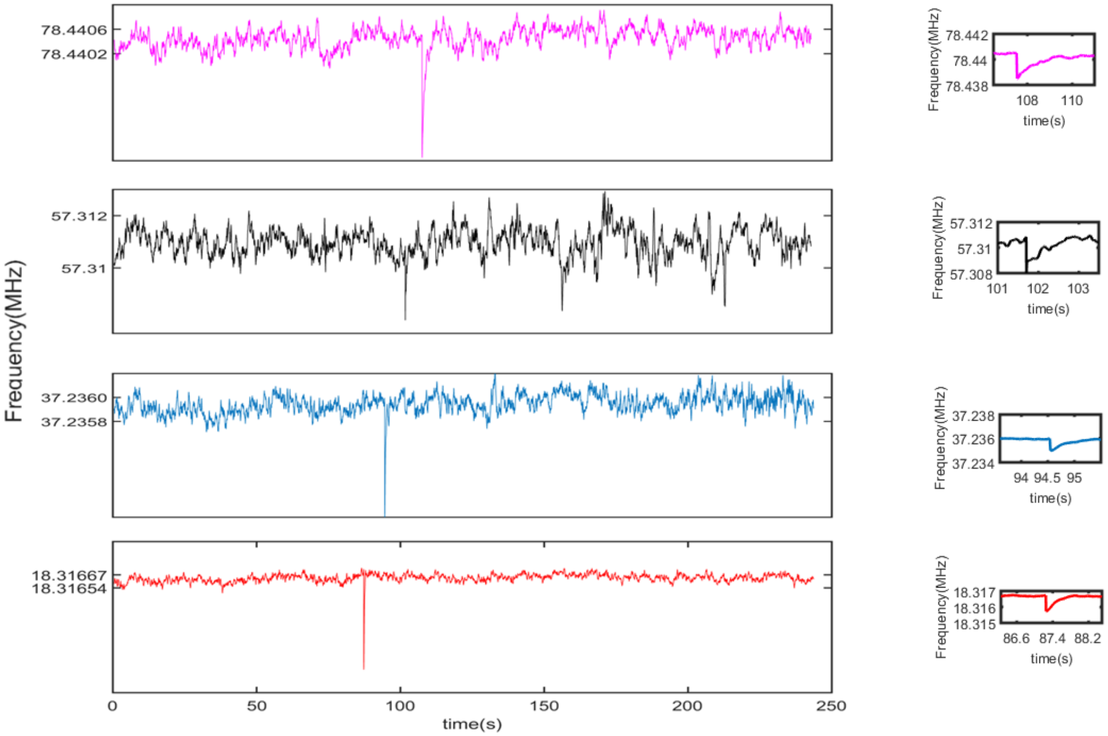

Figure 2.6: PLL response to stimuli and PLL response time are presented.Stimuli are applied simultaneously to see the time they go back to resonance frequency

2.4 Allan Deviation and Mass resolution

Allan deviation is a quantity that shows frequency stability of systems in the existence of noise and drift. In order to determine mass resolution, Allan deviation,$\sigma(\tau)$, must be considered. It can be calculated for different integration times and optimal time to reduce the noise can be chosen.

Allan deviation is the square root of the Allan variance. Allan variance is formulated as

$$\sigma(\tau)^2 = \frac{1}{2(M-1)} \sum_{m=1}^{M} \left(y[m+1] - y[m]\right)^2$$

$y[m]$ is the average value of the fractional frequency difference in the interval m. If we have N data points in total and sampling time of τ_{sample}, we can slice total N data points to M subunits as $a = \frac{N}{M}$, where $\tau = a\tau_{sample}$. As seen in the formula, Allan variance is calculated by taking the difference of two adjacent data points. Therefore, long term drifts will not be so important in the variance of short time periods. In order to measure Allan deviation, resonator should be tracked in resonance frequency over a sufficiently long time. Since device is driven its four vibration modes simultaneously during PLL run, Allan deviation should be measured while each mode is actuated at the same time so that their correlations are also taken into account.

$$\frac{\Delta f}{f} \approx \sigma_A(\tau) \tag{2.2}$$

Mass resolution depends on allan deviation and effective mass of the resonator:

$$\Delta m \approx 2M_{eff}\sigma_A(\tau) \tag{2.3}$$

According to this equation, considering that an analyte lands on the antinodes of the beam ,mass resolution of the device depends on effective mass of the device and Allan deviation. In order to be able to sense lighter particles, it is necessary to reduce have better frequency stability in the measurement and to have lighter resonator.

Chapter 3

ESI and NEMS Mass Spectrometry

3.1 Introduction

Nanoelectromechanical systems are highly sensitive to adhered species and by using NEMS resonators, it is possible to perform NEMS-MS where not only the inertial mass of the molecules but also the position of the adhered particles can be found out by resolving the adsorbate-induced frequency shifts in the first two modes [16, 17, 32].

$$\frac{\Delta f}{f} = -\frac{\Delta m}{2M_{eff}}\phi(x_o)^2 \tag{3.1}$$

By solving the equation above for the first and second modes of the resonator, both mass and position of the accreted particle can be found. When the particle hits the point where there is maximum deflection, it is possible to determine the approximate mass value by considering the relation $\Delta m \approx 2M_{eff}\sigma_A$

Apart from conventional mass spectrometry, NEMS-MS is not based on mass to charge ratio. NEMS resonators determine the inertial mass of the adhered particles.Mass to charge ratio is measured for molecules less than 100kDa accurately with conventional mass spectrometry[33]. It gets harder to measure larger

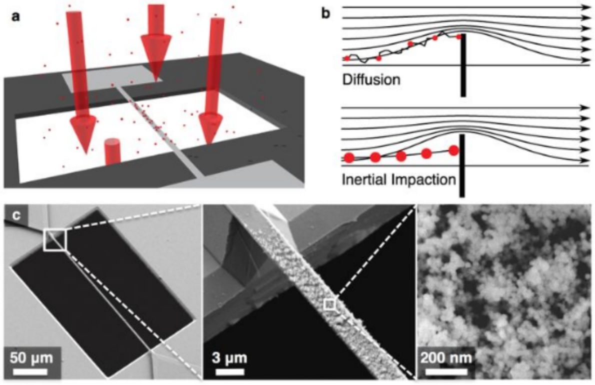

Figure 3.1: Schematic drawing and SEM images of nanomechanical filter fiber. Image is recreated from [34].

molecules by conventional mass spectrometry.

One recent study(Figure 3.1) showed the possibility of collecting and detecting single airborne nanoparticles streamed through resonators and particles are captured by 50μm long 1240 nm wide and 100 nm thick and 138 μm long, 3μ m wide, 220 nm thick silicon nitride coated with a layer of 50nm Al filter fibers in real time. Experiments were conducted in ambient pressure.[34]

Here our primary purpose was to fabricate downscaled version of this filter-fiber resonator and drive the resonator in first two out of plane modes in order to obtain the mass and position information of single 20 nm gold nanoparticles in real time by using two modes theory. For this purpose, we aimed to fabricate NEMS resonator etched from the backside with anistropic KOH etch as in the fabrication of filter fiber.While air molecules flow through the channel, heavy gold particles will not track the flow profile and hit the vibrating NEMS resonator, therefore they will create shifts in resonance frequency.

Experiments started with the NEMS resonators whose fabrication steps were explained in the chapter 2. Thermoelastic actuation and piezoresistive detection is the transduction method of our resonators and we tried to to deliver gold nanoparticles towards NEMS resonator with ESI. Experiments were conducted in around ambient pressure.

3.2 Experimental Setup

Experiments were conducted inside 304 Stainless steel KF 40 Tee. SMA ports were mounted to the blank KF flanges after drilling five holes and it was used to close one side of the tee. PCB on which NEMS chip is wirebonded were placed inside the tee. One side of the tee was connected to SH 110 Scroll Pump and one side was used for SMA feedthroughs and the other side was used for delivery of nanoparticles with ESI. Syringe pump was used to deliver the solution towards the capillary tip.

As indicated in the first chapter, high voltage is applied between the capillary tip and ESI needle to start the process of cycles of evaporation. When the solution goes out from the blunt needle, Taylor cone should be formed. Voltage and distance between capillary tip and needle was arranged to obtain Taylor cone and fine jet for creation of ions. Electrical field between the needle and capillary tip was generated with EMCO E60 High Voltage DC converter. Positive voltage is applied to the ESI needle and negative voltage is applied to the capillary tip which was 1.59×0.36 mm (ODx ID) in diameter(Borşen).

Solution for ESI consists of 500μl gold nanoparticles, 10μl ascetic acid and 500μl methanol. Flow rate of the syringe pump was arranged to achieve a stable Taylor cone, different parameters were tested to achieve it.

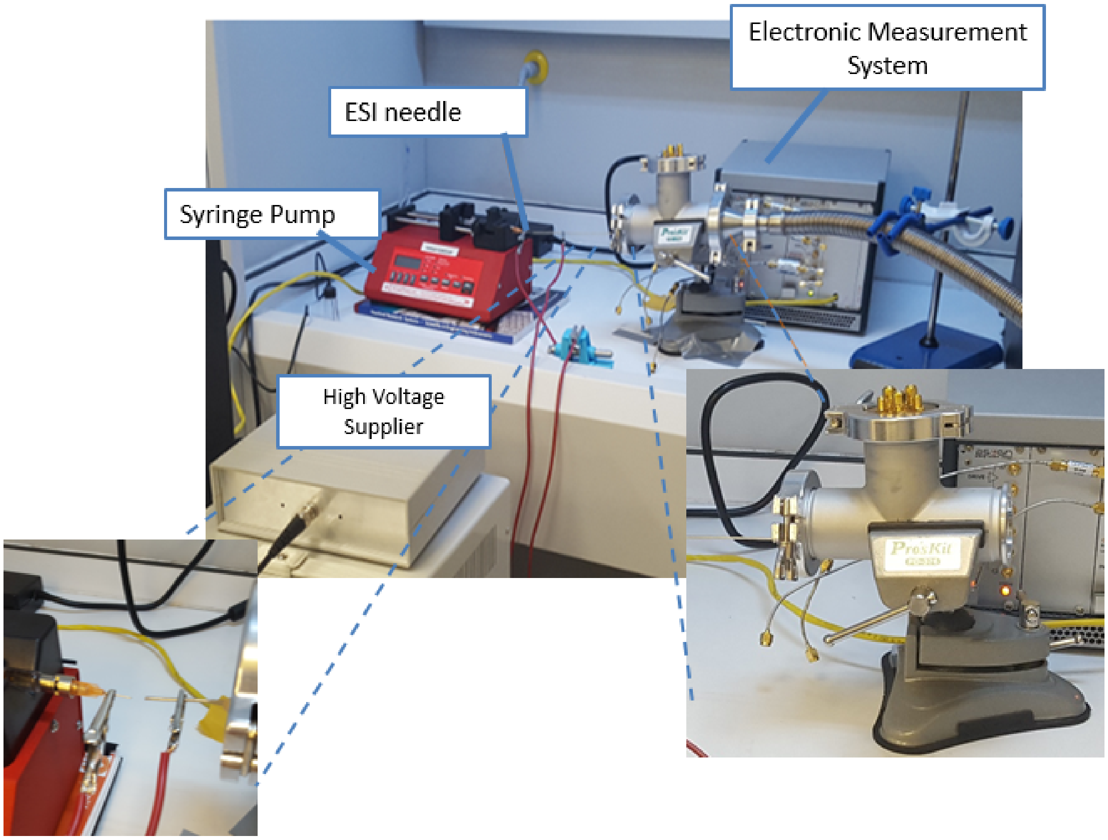

Figure 3.2: Electrospray Ionization Experimental Setup

3.3 GNP Experiments

20-nm gold nanoparticles were tried to measure during the experimental runs. Fabrication steps of the NEMS resonator was the same with the steps explained in chapter 2. Mass of the NEMS used in these experimental runs was about $2.32 \times 10^{-15}\ kg$. Effective mass for the first mode and the second mode should be calculated for the dynamic mass range and we need to consider the frequency stability of the system as well.

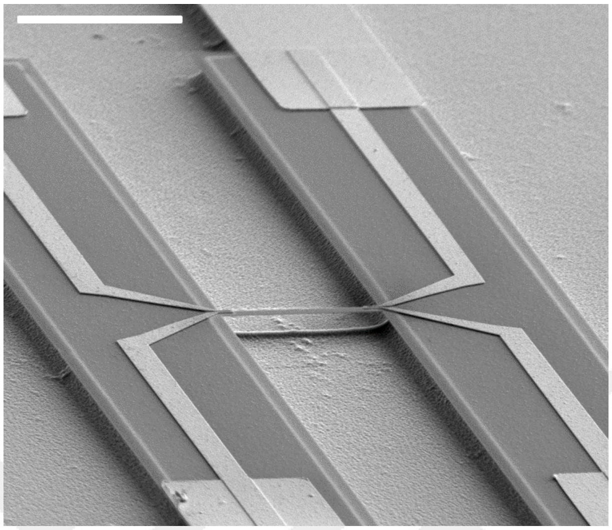

Figure 3.3: NEMS resonator used for the ESI experiments. Scale bar is 10μm

Table 3.1: Necessary parameters to check the dynamic mass range

Mass Resolution	1st Mode	2nd Mode
Allan Deviation	2×10^{-5}	10^{-5}
Effective Mass	$9.24 \times 10^{-16} kg$	$1.02 \times 10^{-15} kg$
Dynamic Mass Range	$22MDa$ <m< $55GDa$	$12MDa$ <m< $61GDa$

First mode was noisier than the second mode so as it is seen in the table 3.1, allan deviation of the first mode was higher. In order to test the resonator, we applied a physical stimuli to the NEMS device. In the figure 3.5, we show the response of the resonator when water-vapor arrives to the beam surface. There is an ubrupt frequency shift in both modes due to mass effect. Throughout the PLL runs for GNPs, we could not observe any shift in resonance frequencies. The reason could be the position of the NEMS resonator. While vacuum pump pulls the molecules, they needed to land on the beam. However, since flow profile and NEMS resonator was placed in paralel, it was hard to direct them to the beam. Therefore we decided to fabricate NEMS resonators etched through the wafer from the backside with KOH etch.

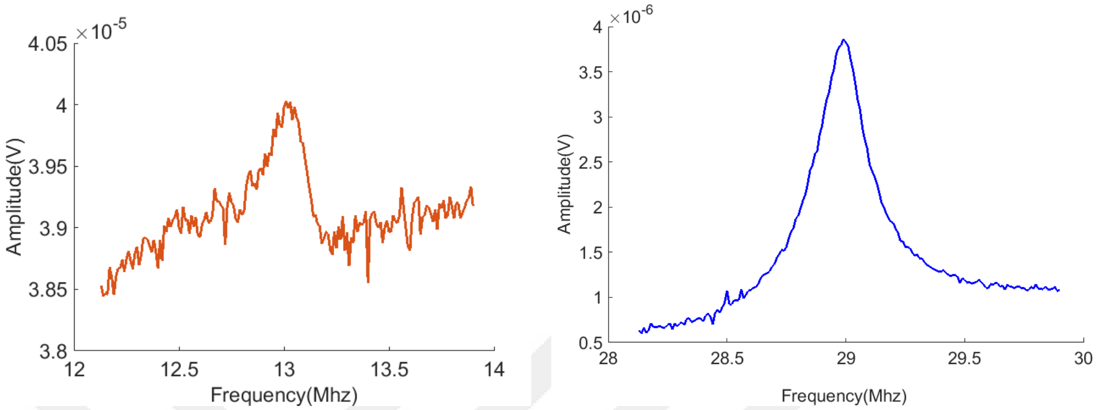

Figure 3.4: 1st and 2nd Mode Open loop Sweeps

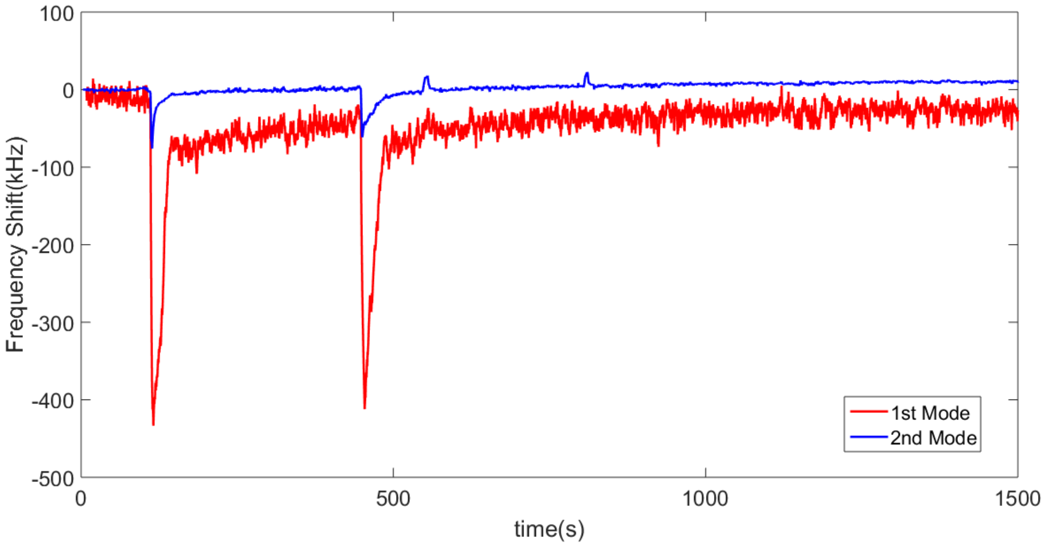

Figure 3.5: During a PLL run, NEMS response was tested to a physical stimulus.Water vapor was sent to the surface of the device through the capillary.

3.4 Fabrication of KOH etched NEMS Resonator

In this process, we aimed to fabricate doubly clamped beam which is around 10μm long. Etch selectivity Si/Si_3N_4 is better than 10^4in 7 M KOH at 80°C[35]. Therefore, Si_3N_4 is used as a an etch mask to etch Si layer.In order to obtain the desired dimension, the concentration and temperature of the KOH solution was optimized after extensive trials.

The wafer was etched in 120gr KOH: 180 ml water at 80°C. Since 500 um thick silicon needs to be etched, this process takes around 14-15 hours. Chips diced out of the low stress double layer Si_3N_4 wafer was exposed to UV light and chip started to be etched in KOH solution. In order to obtain uniform results there are important points to do:

- Temperature of the solution should be stable and in order to do that, a hot plate having a temperature controller unit was used.
- The amount of water should be stable. Water evaporates during the process, thus we must add water once in a few hours to keep the concentration constant.

Fabrication flow of the resonator etched by KOH are explained in figures below.

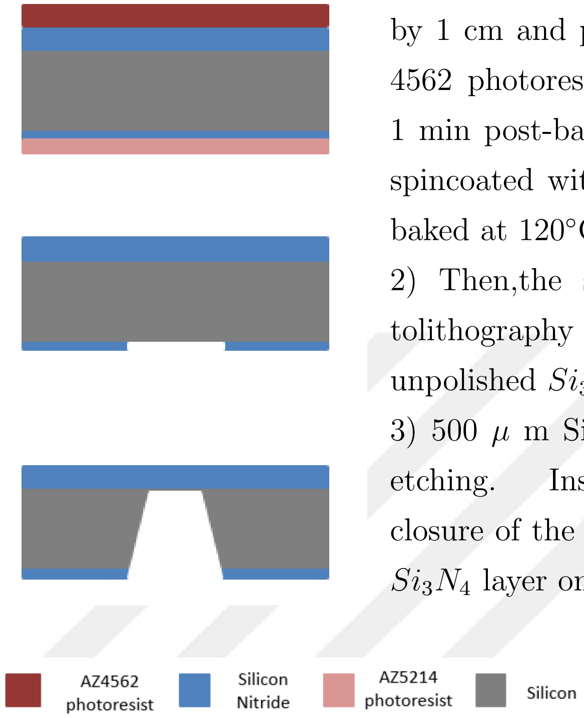

1) Double sided Si_3N_4 wafer was diced 1 cm by 1 cm and polished side was coated with AZ 4562 photoresist to protect the surface. After 1 min post-bake at 110°C, unpolished side was spincoated with AZ 5215, then photoresist was baked at 120°C on the hotplate.

2) Then,the sample was ready for the photolithography step. After the development, unpolished Si_3N_4 layer was etched at ICP

3) 500 μ m Si layer was etched by KOH backetching. Instability in temprerature causes closure of the etch window before it reaches the Si_3N_4 layer on the top.

Fabrication of this device was highly tedious. Up to the point we fabricated the membrane around 10 μm in length, the process was required lots of trial. After we fabricated membranes on the chip, the rest of the steps are not different from the processes explained in the previous chapter. However, doing E- beam lithography on the membrane was critical in terms of alignment. Since we wanted to have a beam at the end of the process, the electrodes should have been aligned well around the membrane.

4) After two E-beam lithography and metallization processes, gold contact pads appeared on the chip.

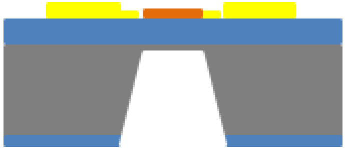

5) 60nm thick Copper layer was deposited.In order to prevent thermal stress, samples dhould be lefts at least one hour after evaporations.

6) After anisotropic Si_3N_4 etch, Cu layer was removed with wet etching.

🟨 Gold
🟦 Silicon Nitride
🟧 Copper
⬛ Silicon

NEMS resonator was fabricated and SEM images are shown in figure3.6 however, when before the wirebonding step we realized that the resistances of the device was very high, showing that they were burnt out. We associated this with EBL process. The last EBL process was on 100 nm Si_3N_4 layer and electrons are bombarded during writing, so this might have caused gold electrodes to burn out. Solution for this problem is to locate the gold electrodes outside of the membrane and Si could be etched in ICP in order to totally suspend the resonator.We have not tried this though and decided to use the devices whose fabrication was explained in chapter 2 in the NEMS-MS with MALDI.

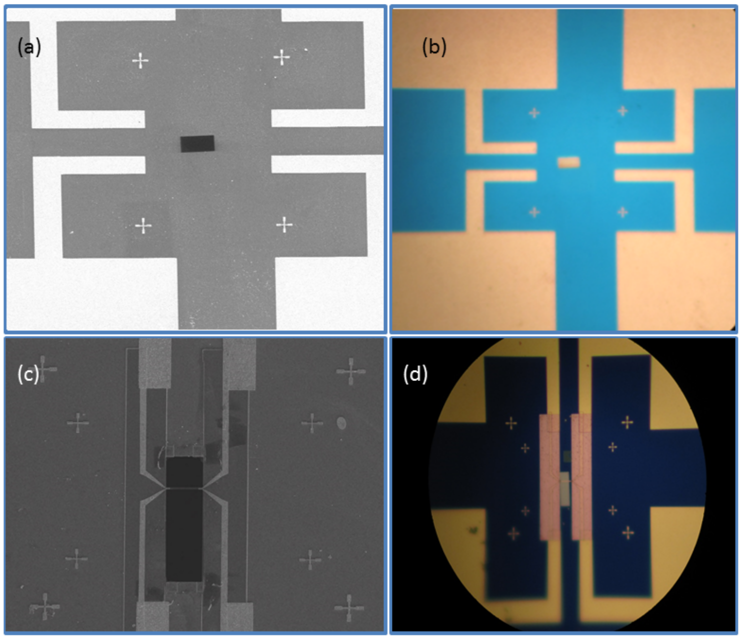

Figure 3.6: Photographs of KOH etched NEMS resonator fabrication Processes (a)SEM image of the sample after EBL of KOH etched Si_3N_4 membrane.(b)Optical Microscopy image of the sample after EBL of KOH etched Si_3N_4 membrane. (c) SEM image of KOH etched NEMS resonator.(d) Optical Microscopy image of NEMS resonator after deposition of Cu mask for ICP etch

Chapter 4

Mass and Stiffness Spectrometry with MALDI

4.1 Introduction

Nanoelectromechanical systems are highly sensitive to adhered species and by using NEMS resonators, it is possible to perform NEMS-MS where not only the inertial mass of the molecules but also the position of the adhered particle can be found out by resolving the adsorbate-induced frequency shifts in the first two modes [17, 32]. Another study wherein experiments were conducted with microcantilever resonators[19] has shown that it is possible to obtain stiffness value of the adsorbate in addition to mass value and position on the beam by using resonance frequency shifts obtained from three mechanical modes.

In our study, double-clamped beam is driven with thermoelastic actuation and vibration is detected with piezoresistive detection to access and measure first four out-of-plane mechanical modes at the same time for real-time study of the adsorbates.

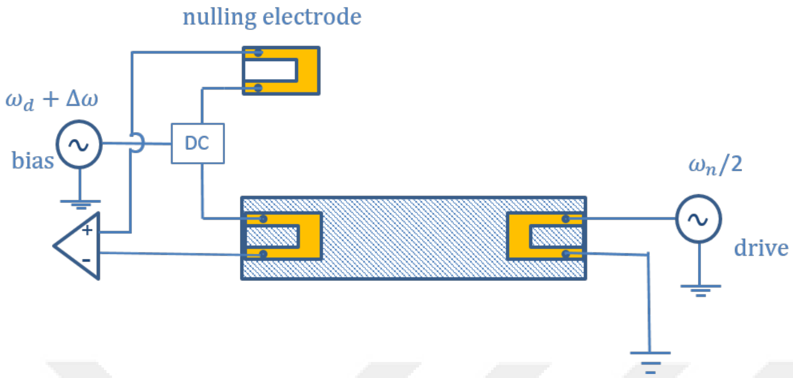

Figure 4.1: Schematic of NEMS circuit, Dbox differential amplifier and nulling electrode are for cancelling the background voltage in NEMS read-out

Adsorbed analytes result in different frequecy shifts since each mode is affected by the perturbations differently. By using normalized frequency shifts,inertial imaging can be implemented for soft analytes thus,multimode information can provide shape properties of analytes [20, 36].Dimensions of the NEMS resonator used in this study are $15\mu m \times 370nm \times 100nm$. There are pros and cons in length of the beam. While length of the beam increases, the capture area for analytes to land on increases as well, however, increase in mass reduces the minimum possible measurable analyte mass since mass resolution depends on effective mass of the vibrating structure. Gold electrodes used in actuation and detection prevent further reduction in width of the beam.

Apart from conventional mass spectrometry, NEMS-MS is not based on mass to charge ratio. NEMS resonators determine the inertial mass of the adhered particles. Mass to charge ratio is measured for molecules less than 100kDa accurately with conventional mass spectrometry[33]. However, heavier biological assemblies can not be measured that accurately with this method. For biological assemblies, NEMS-MS that provides mass sensing with single molecule sensitivity can substitute for conventional MS. As explained in Chapter 1, there are different ways of creating single molecules and we implemented MALDI for molecule delivery towards the NEMS resonator. This method relies on mixing the matrix material and the analyte.Matrices are strong light adsorbands at laser wavelength.They adsorb the energy of the laser and ionizes with analytes. Droplets of the mixture are applied and dried on the glass slide. When glass slide is exposed to laser through a lens, the matrix ionizes the analyte and they spread on the area and sticks to the NEMS device located in front of the slide. There are different alternatives but in this study backside desorption method where laser light is directed to the backside of the glass slide was chosen due to its applicability. Multimode NEMS-MS experiments were conducted for a variety of analytes which are Gold Nanoparticles(GNPs),centrosome organelle obtained from HeLa cells, M13ke bacteriophages. While GNPs does not necessitate different UV absorband matrix in its solution since it behaves as both matrix and analyte, other biological analytes necessitate matrix components.

There are variety of matrix components and they can be divided into two main categories which are solid and liquid matices. Ionic liquid matrix (ILM) that is more advantageous than solid matrices used as a matrix substance in our study. Since it produces homogeneous solutions of matrix and analyte and there is no need to search for hot spots[37]. IMTBA-CHCA is chosen as ILM since it is applicable for protein and peptide analytes. The product purchased from Sigma Aldrich was in the form of powder, thus it was dissolved in ethanol and methanol mixture before mixing with analyte solution.

4.2 Experimental Setup

Multimode NEMS-MS experiments were conducted in table-top UHV capable chamber (Kurt Lesker).The chamber is six way cross and has 6” ID flanges. Experiments were conducted in high vacuum conditions ($10^{-8} - 10^{-9}$ torr) to reduce molecule interactions that may affect the molecule delivery to NEMS resonators negatively. Experimental setup for this study is originated from an earlier work [32] where backside desorption method was implemented. UHV Design Multibase is capable of axial alignment ±22 mm in x and y axes. It works by arranging the position of moving flange according the fixed leadscrews. XY stage has two stepper motors.(McLennan) They were controlled with a PIC microcontroller.

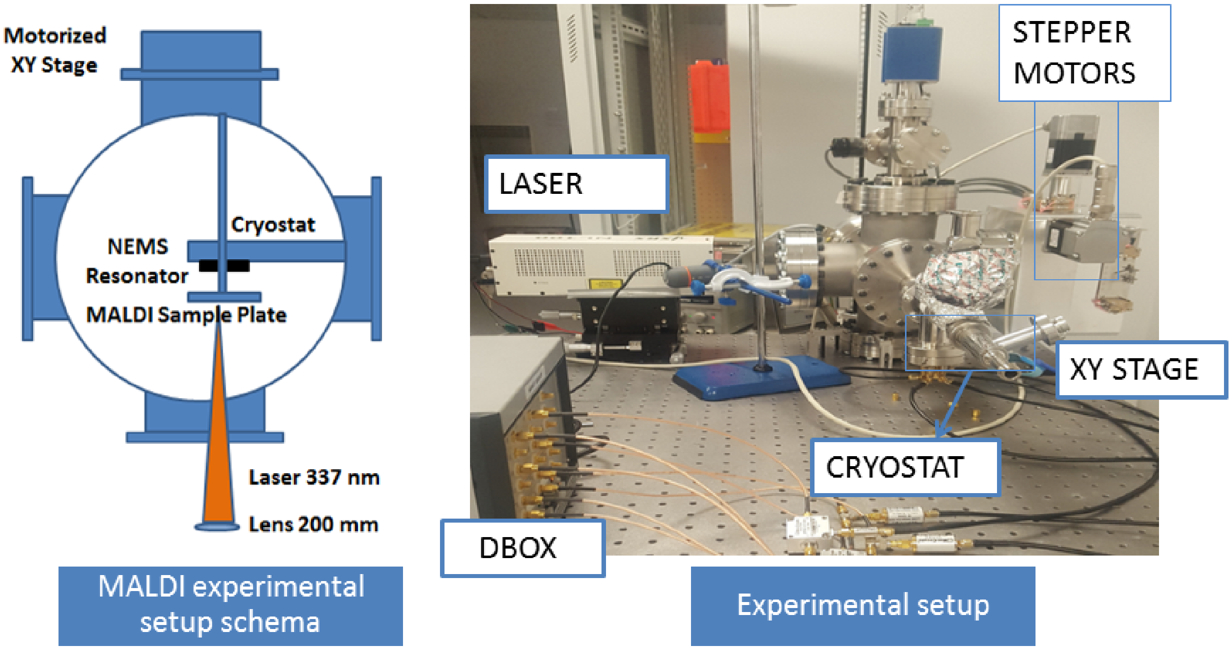

MALDI experimental setup schema

Experimental setup

Figure 4.2: Schema of Experimantal setup from top view and Photograph of Setup consists of Vacuum chamber, flow cryostat, laser and lens, xy stage, stepper motors

In order to perform MALDI, NEMS resonator was mounted on a flow cryostat and the cryostat (Janis) was placed inside the chamber. MALDI sample plate was arranged in parallel to NEMS resonator with the help of an aliminum part. This part was hanged on an arm mounted on X-Y stage used in order to scan the surface of the glass slide and to find the hot spots. The flow croyostat allows the NEMS resonators to cool down up to cryogenic temperatures.In our experiments liquid nitrogen cooled the system to 77 K.Cooling the device provides physisorption and reduces the fluctuations in frequency, so MALDI experiments for GNPs and some of the data for centrosome experiments were conducted in low temperatures. After we realized that Allan deviations at room temperature and cryogenic temperature did not differ too much (not in order of magnitude level) in our resonators for some reason that can be related with NEMS resonators and electronic equipments, we decided to continue experiments for soft analytes at room temperature.

NL 100 nitrogen laser (Stanford Research Systems) was used to perform MALDI. It has 337 nm wavelength and 176 $\mu J/pulse$ laser energy.Since it has a rectangular beam, laser focusing lens is necessary to increase its energy and direct it to a point. Laser focusing lens (200mm) was mounted in front of the laser beam shutter and NL 100 was placed on XYZ micrometer stage in order to arrange laser beam towards NEMS resonator.

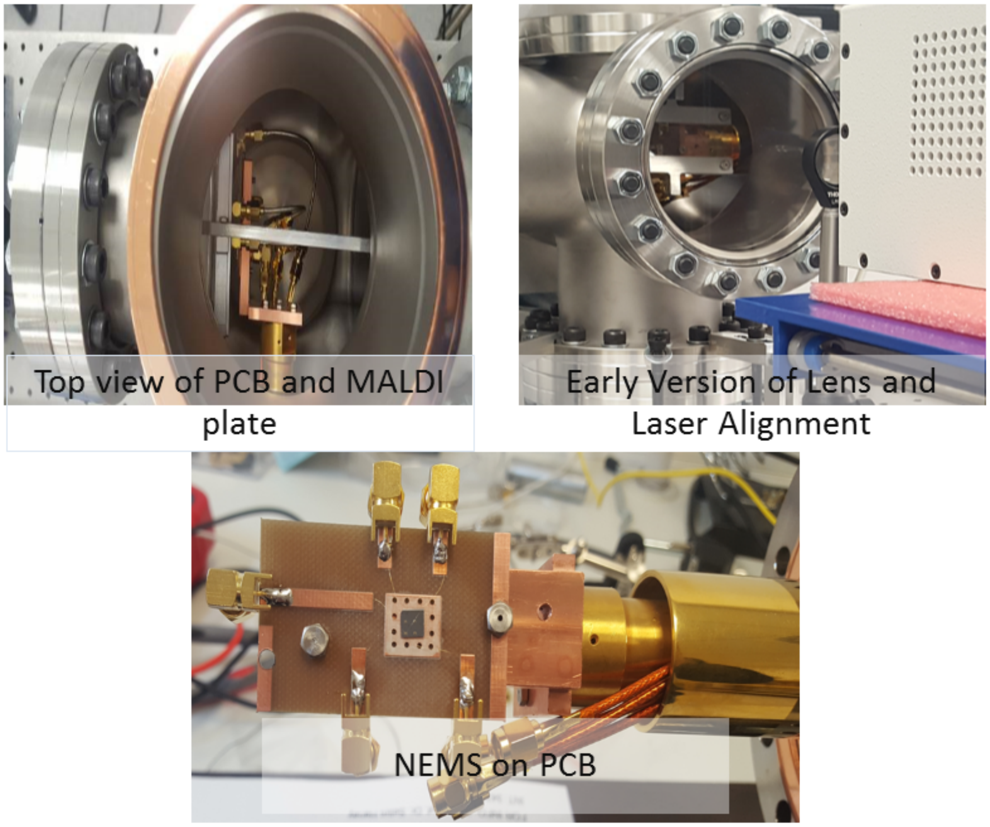

Figure 4.3: Construction of experimental setup consisting of vacuum chamber, NEMS PCB, laser and 20 cm-lens.NEMS PCB was mounted on a copper plate in order to provide conduction during cooling

NEMS resonator was located in the middle of a PCB and MALDI plate was placed approximately 5-6 mm away from NEMS resonator. A glass flange was used to allow laser light to be directed towards NEMS. It is critical to assure that laser beam is directed to NEMS device. When it is done, NEMS resonance frequency which is locked by PLL starts to decrease due to laser energy. This shows that it is in correct position. After a while resonance frequency stabilizes. As stated in chapter 3, DBOX channels can be operated at the same time for multimode drive and detection.Each channel has a dual tone option in addition to single tone. Therefore, by using two channels it is possible to actuate the NEMS resonator in four different mechanical modes simultaneously. For measurement of Allan deviation, data set is parsed into different intervals and Allan deviation is measured for each interval.The value corresponding to PLL response time gives us Allan deviation. Mass resolution is the lower bound that we can measure with the NEMS MS. If we think that the particle adhered to the antinode of the mode, we will have the relation:

$$\delta m \approx 2m_{eff}\sigma(\tau)$$

As we see, mass resolution depends on allan deviation and effective mass. Mass of the device is about 1.82 x $10^{-15}kg$. Effective mass correction factors for the first four modes and allan deviations in 77 K are written in the table below.

Table 4.1: Mass Resolution

Modes	Effective Mass Correction	Allan Deviation (@77K)	Mass Resolution (MDa)
1st Mode	0.3964	7×10^{-7}	0.6
2nd Mode	0.4389	1×10^{-6}	0.96
3rd Mode	0.4370	7.5×10^{-6}	0.72
4th Mode	0.4371	7×10^{-7}	0.67

Resonance frequencies and quality factors of four out of plane mechanical modes before and after experiments are shown in the graphs of Lorentzian fits to X-Y quadrature. It is clear that resonance frequencies drop due to particle adsorption.

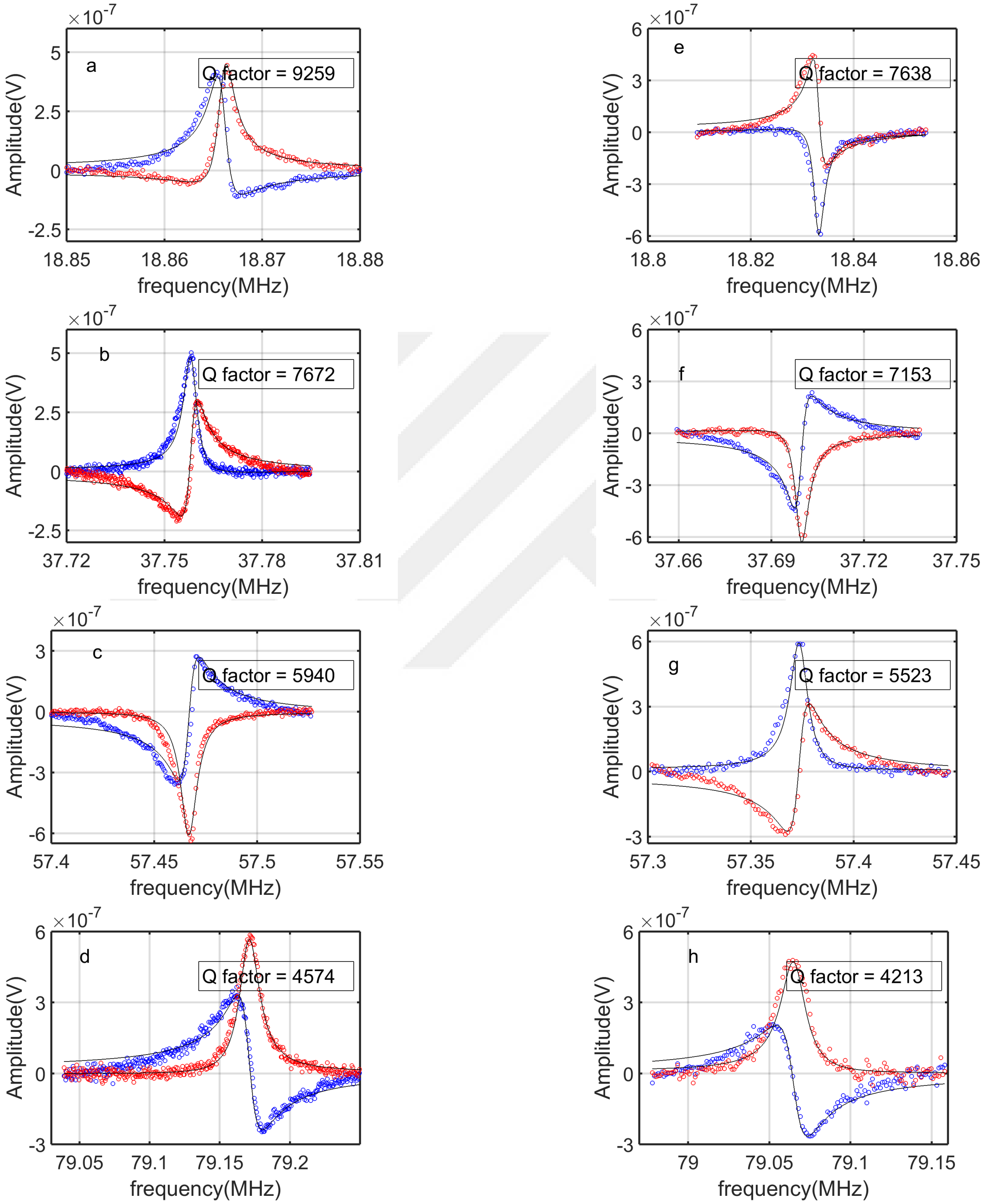

Figure 4.4: X and Y quadratures of four vibration modes before MALDI experiments and after MALDI experiments

4.3 Statement of the Problem

As the number of the simultaneous vibration modes in the detection increases, it is possible to measure position, mass and size of adsorbates. The theory of inertial imaging can be found elsewhere[20, 32, 36]. Since inertial imaging theory is applicable for soft analytes and frequency shifts obtained from four vibration modes cannot provide accurate shape properties for GNPs. As indicated before, we obtained frequency shifts for four vibration modes of the NEMS resonator and our purpose is to obtain mass, stiffness and shape spectrometry for analytes used in the experiments .

Inertial imaging theory asserts that mass, position,size and shape information of soft analytes can be obtained through multimode detection.This approach goes beyond the point mass approximatioan and provides the possibility of image reconstraction as a result of spatial moments of mass distribution[20, 36]. Inertial Imaging Theory however, does not take stiffness of the analyte into consideration by relying on the fact that stiffness of the soft analytes are so small when compared with the stiffness of the beam. This effect is not negligible for GNPs as in the case of soft analytes since GNP stiffness is comparable with beam stiffness.Here we develop a theory that combine stiffness and size effects.

4.3.1 Theoretical Calculations

Inertial Imaging Theory that gives spatial extent of soft adsorbates were simplified recently and in this theory, it was shown that multimode measurements offer characterization of shape information by going beyond of point - mass approximation. This framework will be an improvement to inertial imaging theory and it will offer stiffness of GNPs in addition to position and mass values by assuming that adsorbates are hemisphere.

Under the light of Euler-Bernolli Beam Theory, we are going to calculate strain and kinetic energy of the beam and particles per oscillation and by equating those energies we are going to obtain resonance frequency of doubly clamped beam.

When the resonator vibrates, the strain occurred on the beam can be expressed as below.

$$\varepsilon_{xx} = -(y + \frac{h}{2})\frac{d^2w}{dx^2} \tag{4.1}$$

where $w\left(x\right) = A_n\varphi_n(x)$.

Strain energy is in general equals to:

$$U = \frac{1}{2}\iiint E{\varepsilon_{xx}}^2 dV \tag{4.2}$$

By assuming that gold nanoparticles are hemishpere, from (4.1) and (4.2) strain energy of a particle on the beam and strain energy of the beam result in the following equations:

$$U_p = \frac{1}{2}\ {A_n}^2\ \left[E_a\left(\frac{\pi h^2 r^3}{6} + \frac{\pi h r^4}{4} + \frac{2\pi r^5}{15}\right){\varphi_n}''{(x_0)}^2\right] \tag{4.3}$$

$$U_b = \frac{1}{2}{A_n}^2 E_b\ I_b \int_0^L {\varphi_n}''{(x)}^2 dx \tag{4.4}$$

Kinetic energy of the beam and particle will be calculated as :

$$T_b = \frac{1}{2}\ {A_n}^2\ {\omega_n}^2\rho_b V_c\ \int_0^L {\varphi_n}^2(x)dx \tag{4.5}$$

$$T_p = \frac{1}{2}{A_n}^2\ {\omega_n}^2\int_0^L \mu(x){\varphi_n}^2(x)dx \tag{4.6}$$

Taylor expanding ${\varphi_n}^2(x)$ around x_0 , position of the analyte, will give us the equation below

$$T_p = \frac{1}{2}{A_n}^2\ {\omega_n}^2\left[\rho_p\ V_p\varphi_n\left(x_0\right)^2 + \sum_{p=2}^{\infty}\frac{1}{p!}\frac{\partial^p\varphi_n(x)}{\partial x^p}\bigg|_{x=x_0}\int_0^L \mu(x)(x-x_0)^2\right] \tag{4.7}$$

For ease of calculation, we will only include the term $p = 2$ and this will decrease complexity of the problem and $\mu(x)$ is again calculated with hemisphere assumption.

$$T_p = \frac{1}{2}{A_n}^2\ {\omega_n}^2\left[\rho_p\ V_p\varphi_n\left(x_0\right)^2 +\ \alpha\left(\left(\frac{\partial\varphi_{n(x)}}{\partial x}\bigg|_{x=x_0}\right)^2 + \varphi_n(x_o)\frac{\partial^2\varphi_n(x)}{\partial x^2}\bigg|_{x=x_0}\right)\right] \tag{4.8}$$

Size effect is going to be scaled with α and for hemisphere, it is going to be:

$$\sigma = \frac{2\pi r^5 \rho_p}{15}$$

Eigen functions are normalized such that the equation below is satisfied

$$\int_0^1 {\varphi_{n(x)}}^2 dx = 1$$

where $x = \frac{x}{L_b}$, normalized by the beam length. Normalization in mode shape is going to change the equations as below

$$U_p = \frac{1}{2}\ \frac{{A_n}^2}{L_b^4} \left[E_a \left(\frac{\pi h^2 r^3}{6} + \frac{\pi h r^4}{4} + \frac{2\pi r^5}{15} \right) {\varphi_n}''(x_0)^2 \right] \tag{4.9}$$

$$U_b = \frac{1}{2} \frac{{A_n}^2 E_b\ I_b}{{L_b}^3} \int_0^1 {\varphi_n}''(x)^2 dx \tag{4.10}$$

Kinetic energy of beam will be

$$T_b = \frac{1}{2}\ {A_n}^2\ {\omega_n}^2 \rho_b V_b\ \int_0^1 {\varphi_n}^2(x) dx \tag{4.11}$$

And particle kinetic energy will be

$$T_p = \frac{1}{2} {A_n}^2\ {\omega_n}^2 \left[\rho_p\ V_p \varphi_n\,(x_0)^2 +\ \frac{\sigma}{{L_b}^2} \left(\left(\frac{\partial \varphi_{n(x)}}{\partial x}\Big|_{x=x_0}\right)^2 + \varphi_n(x_o) \frac{\partial^2 \varphi_n(x)}{\partial x^2}\Big|_{x=x_0} \right) \right] \tag{4.12}$$

In order to find resonance frequency, potential and kinetic energies per oscillation cycle should be equal[38].According to Rayleigh Ritz Theorem, resonance frequency of the beam for unloaded case is equal to:

$${\omega_n}^2 \approx \frac{E_b\ \ I_b \int_0^1 {\varphi_n}''(x)^2 dx}{\rho_b V_b {L_b}^3\ \ \int_0^1 {\varphi_n}^2(x) dx} \tag{4.13}$$

When a particle lands on the beam, new resonance frequency of the resonator will be

$$\omega_n{}^2 \approx \frac{\frac{E_b \quad I_b}{L_b{}^3} \int_0^1 \varphi_n{}''(x)^2 dx + \left[\frac{E_p}{L_b^4}\left(\frac{\pi h^2 r^3}{6} + \frac{\pi h r^4}{4} + \frac{2\pi r^5}{15}\right)\varphi_n{}''(x_0)^2\right]}{\rho_b V_b \quad \int_0^1 \varphi_n{}^2(x) dx + \left[\rho_p \quad V_p \varphi_n(x_0)^2 + \frac{\sigma}{L_b{}^2}\left((\frac{\partial \varphi_{n(x)}}{\partial x}\Big|_{x=x_0})^2 + \varphi_n(x_o)\frac{\partial^2 \varphi_n(x)}{\partial x^2}\Big|_{x=x_0}\right)\right]}$$

At this point, we need to find $\Delta f_n/f$ and in order to make our calculations easier, we used the approximation below which was obtained after applying Taylor series expansion[26]:

$$\frac{\omega_{no}}{\omega_n} \approx \frac{1}{2}\left(\frac{U_p}{U_b} - \frac{T_p}{T_b}\right) \tag{4.14}$$

After arranging the equation, we obtained the relation below.

$$\frac{\Delta f}{f} \approx \frac{6 E_p V_p}{E_b V_b}\left(\frac{1}{4} + \frac{3r}{8h} + \frac{1}{5}\left(\frac{r}{h}\right)^2\right)\frac{\varphi_n{}''(x_0)^2}{\int_0^1 \varphi_n{}''(x)^2 dx} - \frac{1}{2}\frac{V_p \rho_p}{V_b \rho_b}\left(\varphi_n(x_0)^2 + \varphi_n{}'(x_0)\varphi_n{}''(x_0)\frac{r^2}{5 L_b{}^2}\right) \tag{4.15}$$

In the beginning, our purpose was to decouple size, density, stiffness and position of anaytes by using four mechanical modes. To obtain those, we swept values of radius, density, position and Young's Modulus and calculated frequency shifts for each mode using the last equation. Combination of parameters that give the closest values to experimental frequency shifts was accepted as the parameters that we searched for. However, we noticed that the term including square of the radius in kinetic energy does not create a valuable impact in comparison to the other term. With the data we have now, we can not obtain all of those. Therefore, we decided to calculate mass, stiffness and position of analytes on the beam.

We converted the equation 4.15 to linear form and used least square method to find the coefficients of unknowns. Eigen-frequency shifts of three mechanical modes will be enough to obtain them. By implementing these equations in MATLAB, we try to match the experimental and theoretical frequency shifts.

$$\frac{\delta f_n}{f} = x_1 \alpha_n + x_2 \beta_n \tag{4.16}$$

Least square method was used to find α and β values which cover the mode shape related functions in the equation 4.15.The algorithm used to find the unknown parameters is given in the figure below.

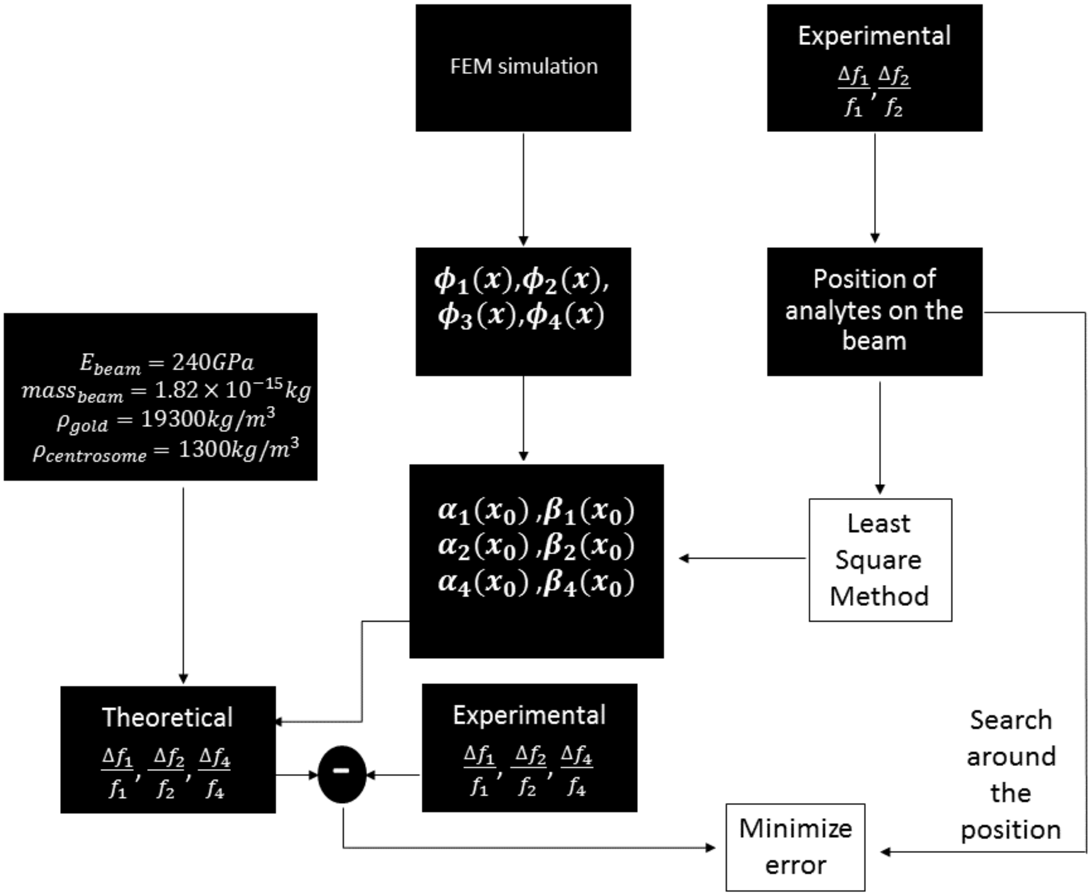

Figure 4.5: Flow Diagram of the Method

4.4 Gold Nanoparticle Experiments

20-nm GNPs purchased from Sigma Aldrich were used in MALDI-based measurements. GNPs behave as matrix and analyte during desorption and ionization therefore there is no need for matrix addition[32, 39]. There is %10 dispersion in diameter of the particles therefore diameters of particles vary between 18 and 22 nm. As explained in Chapter 1, frequency shifts caused by an analyte landed on beam are proportional to the ratio of the its mass to the resonator mass and the proportionality depends on the position of the analyte on the beam[16, 17, 32]. In this study, we used four out of plane modes of the doubly- clamped beam NEMS resonators and frequency shifts of 64 adsorption events were recorded.

During experiments, vacuum pressure was pumped down to around 10^{-9} torr and NEMS resonator was cooled down to 77 K. Additionally, we conducted experiments in room temperatures as well and compared SEM views with the positions obtained from theoretical calculations.

4.4.1 Results of Two Modes Theory

We analysed results by using two modes theory to understand whether they are individual events or uniform deposition on the surface. The normalized shifts of first two modes showed that position spectra for GNPs have a large distribution, therefore they are individual events rather than a uniform deposition.We do not expect a single peak in mass distribution and as seen in mass spectra, some events have very large mass distribution and there may be clustering in size and that is why size variance is much higher than the actual samples.

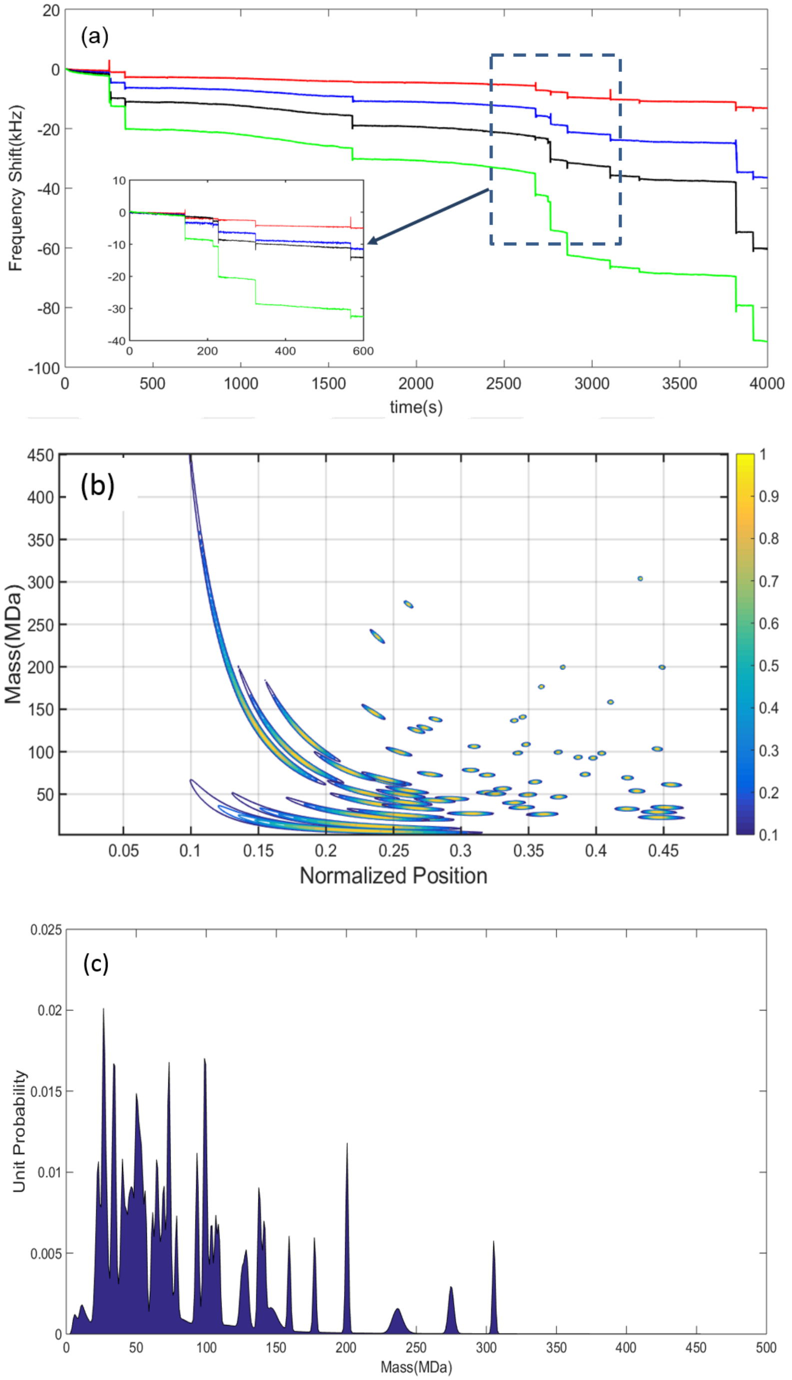

Figure 4.6: (a)Real-time eigenfrequency jumps in first four mechanical modes of doubly clamped beam due 20-nm gold nanoparticles.(b) Joint Probability Distribution of mass and position of adsorption of GNPs (c)The mass distribution of GNPs

Experiments for GNPs were repeated in room temperature as well. We recorded 19 data in PLL measurements and 21 nanoparticles were observed under the SEM. We tried to match SEM and theoretical results. Position values of GNPs in sweet area match well with the results of two modes theory. It is hard to detect the particles landing near the clamping points and half of the resonator.

Table 4.2: Comparison of Positions from SEM View and Two Modes Theory

Event No	fjump1$\times 10^4$	fjump2$\times 10^4$	Positions from Theory	Positions from SEM
1	1.402	2.960	0.2412	0.248
2	2.444	0.4992	0.4274	0.435
3	2.727	3.168	0.3186	0.323
4	2.456	3.207	0.3064	0.30
5	2.0943	4.4347	0.2406	0.24
6	1.7836	2.603	0.2936	0.296
7	1.6206	0.4597	0.4142	0.418
8	2.9199	1.1939	0.3964	0.394
9	0.111	0.139	0.311	0.313
10	0.1945	0.6167	0.1505	0.152
11	1.132	1.179	0.3295	0.323
12	1.7265	0.178	0.4487	0.453
13	3.050	4.969	0.2797	0.262

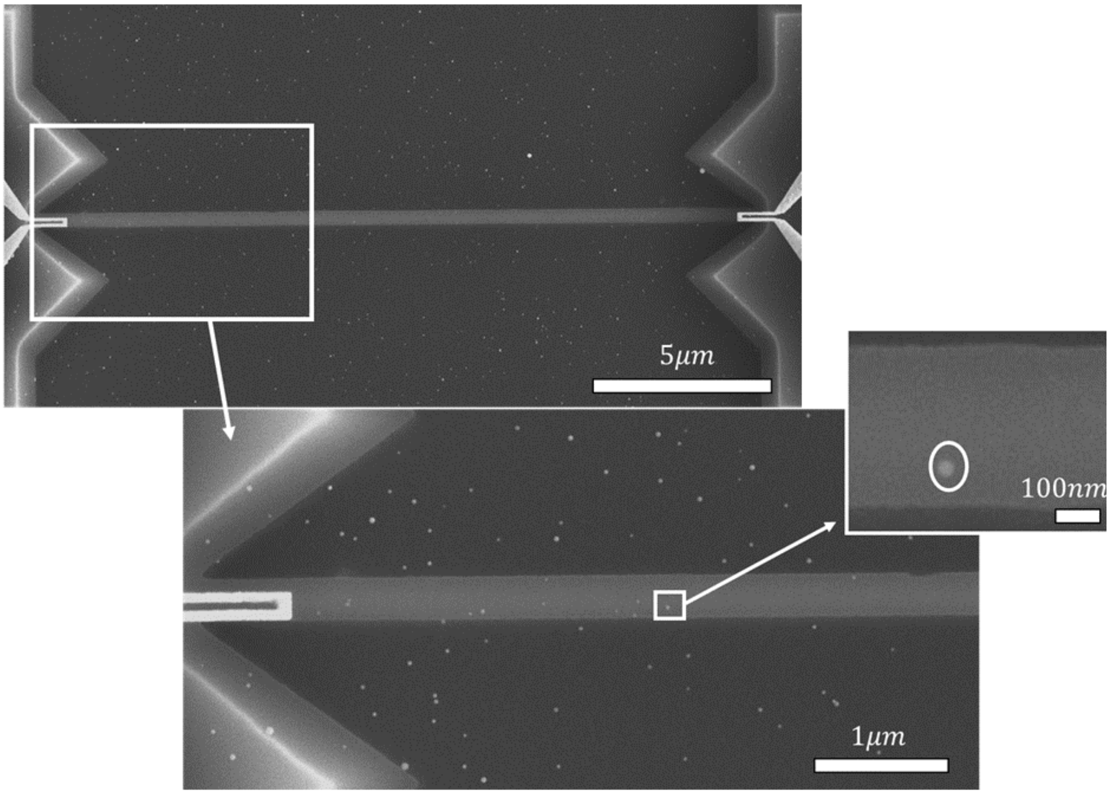

Figure 4.7: SEM image after GNP Experiments

4.4.2 Results of Hemisphere Approximation

We applied our theory wherein we assume that analytes are hemispheres and used an algorithm to minimize the difference between the experimental and theoretical frequency shifts. First, second and fourth mechanical mode shifts were used in the minimization algoritm since they fit better. We saw that it is not possible to decouple size and density of analytes. Due to the nature of the equation we presented, our algorithm tries to keep the mass constant. Another issue is that we need density of nanoparticles to obtain stiffness [19]. Therefore, we took the density of bulk gold which is $19300kg/m^3$ and we could obtain mass and stiffness as below.

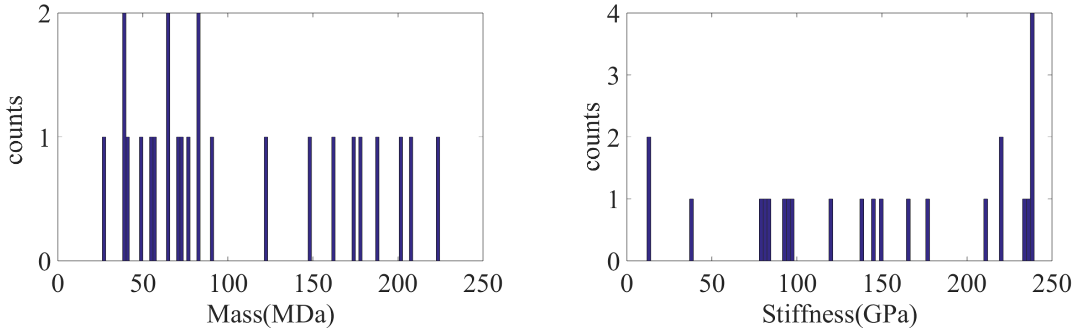

Figure 4.8: Mass and Stiffness values of GNPs data

Outlier data was detected with an statistical approach called ztest and outliers were eliminated. According to our results, mass of nanoparticles are found as 104 ± 62.8 MDa, Young's Modulus was calculated as 148.2 ± 76.6 GPa and radius of GNPs corresponding to the density of $19300 kg/m^3$ are calculated as 15.6±3nm

4.5 Centrosome Experiments

As already stated in Chapter 1, MALDI requires UV absorband in order for analytes to desorb and ionize. There are lots of matrices in literature classified as solid and liquid matices. Solid matrices have advantages of low vapor pressure whereas liquid matrices provide more homogenous solutions in addtion to better shot-to-shot reproducibility[40]. Ionic liquid matrices combine both good properties for MALDI. Due to its convenience for proteins, IMTBA-CHCA(N-isopropyl-N-tert-butylammonium-α-cyano-4-hydroxycinnamate) was selected among ILM alternatives and purchased from Sigma Aldrich.The product is in powder form, therefore we dissolved it in ethanol and methanol mixture, then it was mixed with analyte solution.

Centrosomes are composed of two centrioles made of nine bundles of microtubules and and they are surrounded by pericentriolar material (PCM). Centrosomes obtained from HeLa cells were prepared in Cystoskeleton Research Laboratory in Koç University. They were prepared in $\%50 - 70$ sucrase solution and the number of centrosomes in 1 ml solution was around $60x10^6$. We needed to do buffer exchange to remove sucrase and since its concentration is high, it is better to repeat the procedure 2-3 times.

Table 4.3: MALDI Sample Preparation

1. Centrifuge the centosome and sucrase mixture in 10 kDa filter (stir 2 hours at 3500xg)
2. ILM is dissolved in 300ml ethanol and 100ml methanol solution
3. ILM solution and resultant centrosome solution are mixed together
4. Mixture is deposited on glass slide with the help of micropipette
5. Wait for complete drying

After cleaning the glass slide in acetone and IPA and driying with compressed air, matrix and centrosome mixture were deposited on the glass slide from solution by using a pipette and left for drying in ambient conditions. We tried to conduct our experiments at room temperature and after we saw that we could get eigenfrequency jumps in this condition, we stopped cooling the system. Mass resolution for room temperature experiments are give in the table 4.4.

Table 4.4: Mass Resolution

Modes	Effective Mass Correction	Allan Deviation (@298K)	Mass Resolution (MDa)
1st Mode	0.3964	2×10^{-6}	1.73
2nd Mode	0.4389	1.8×10^{-6}	1.73
3rd Mode	0.4370	1.8×10^{-6}	1.72
4th Mode	0.4371	2×10^{-6}	1.91

4.5.1 Results of Two Modes Theory

Although we detected frequency jumps, they were so rare. One the possible reasons behind this may be that the number of centrosomes deposited on the glass slide is around 10^{-6} and NEMS and probability for an event to occur is low due to small capture area of NEMS sensor. And also, it is possible that matrix salt acquires necessary energy for desorption after a certain number of laser shots and this takes a long time. As seen in the graph, there is a drift in resonance frequencies. This happens when laser is turned on and there was no drift in GNPs experiments, thus this may be because of matrix salt.

The other issue is that as seen in the figure 4.9, the position spectrum of centrosomes accumuleted mostly around 0.33L − 0.37L and the reason of this may be because some events are actually uniform depositions, thus not single molecule adsorptions. When we do not include the data corresponding to the normalized positions around 0.33L − 0.37L, we obtain the mass and position distributions as in the figure 4.10.

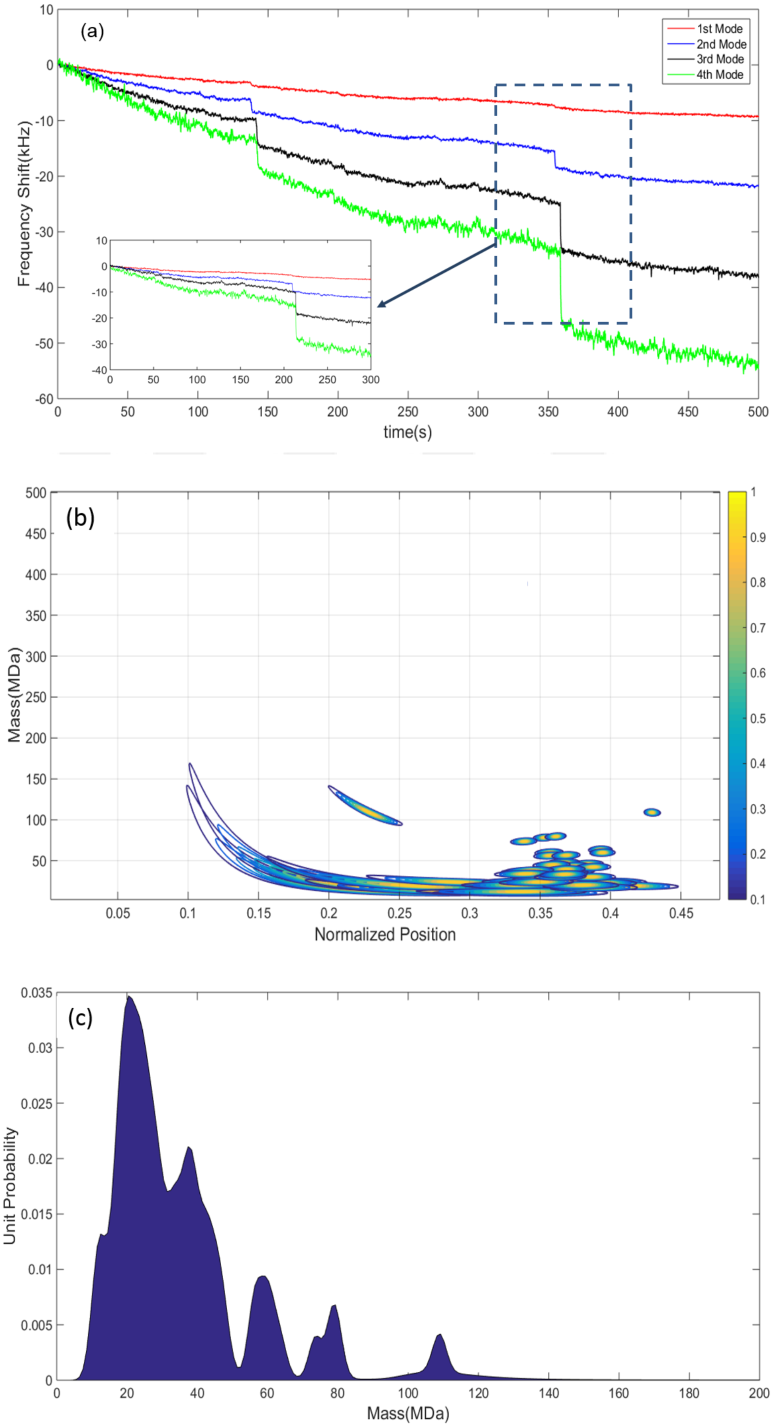

Figure 4.9: (a)Real-time eigenfrequency jumps in first four mechanical modes of doubly clamped beam due to centrosomes.(b) Joint Probability Distribution of mass and position of adsorption of centrosomes (c)The mass distribution of centrosomes.

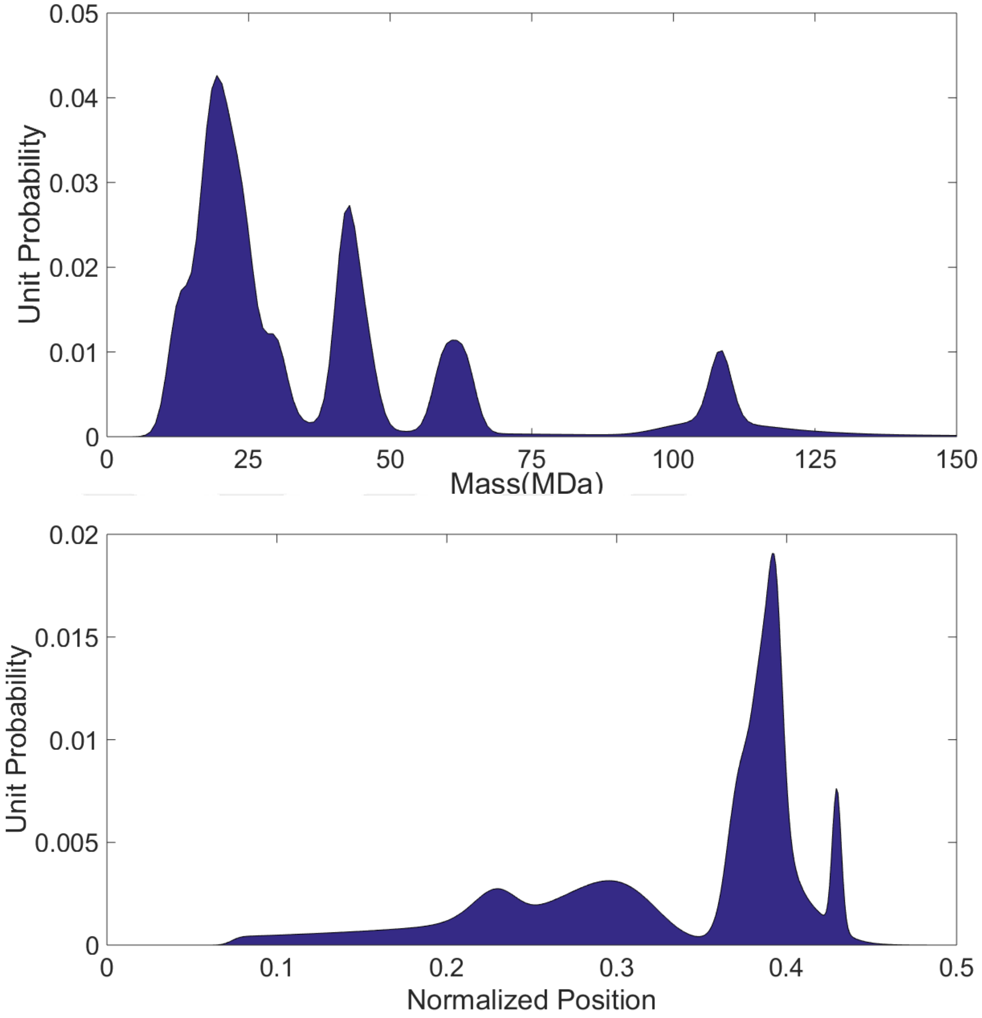

Figure 4.10: Mass and Stiffness values of centrosome data

4.5.2 Results of Hemisphere Approximation

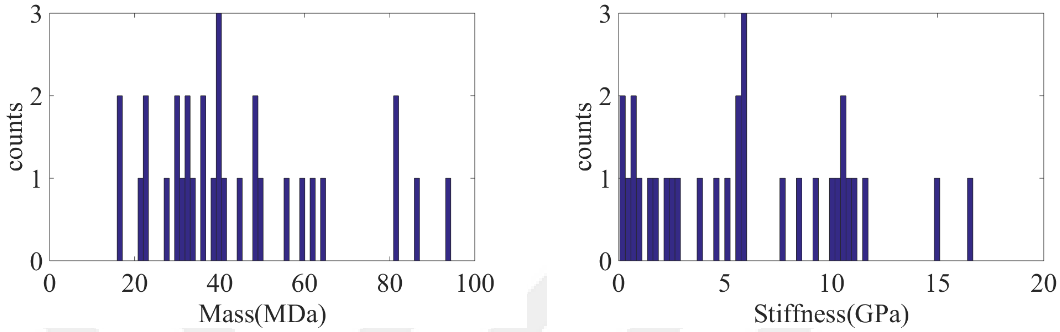

Figure 4.11: Mass and Stiffness values of centrosome data

As in GNP experiments, outliers were eliminated by ztest. The calculations provided mass as 44 ± 20.5 MDa, Young's Modulus as 6 ± 4.6 GPa. Radius of centrosomes with hemisphere approximation was found as 30 ± 4.5 nm. We have taken the density value as $1300kg/m^3$ for calculation of stiffness. As stated in GNP experiments we need density value to calculate the stiffness of analytes. Since we do not know the exact value of the density, this stiffness value may not reflect the real value however, we tried to implement a value close to the density of protein molecules.

4.6 Bacteriophage Experiments

M13ke phages were also tested in the experiments of NEMS based spectrometry.We thought that we can increase the event rate, since phages can be prepared in higher concentration than centrosomes. There were about 10^{12} phages in 1 ml solution. Phage samples were prepared Syntetic Biosystem Lab in National Nanotechnology Center (UNAM). Matrix salt was the same as centrosomes and we applied the same procedure to dissolve it and mixed with our anaytes.

Experiments have been conducted for three days. In contrast with our expectation, we could observe only four frequency jumps in experiments.We tried to decrease the matrix concentration for the next test tubes, however, we could not see any events in new trials. Position of the recorded four data are in the different locations on the beam though. Since we had only a few data, we can not reach a conclusion for their mass and stiffness values. It seems that bacteriophages are not a good candidates for MALDI. ESI or other ionizations methods may work. SEM images shown in the figure 4.13 have some structures near the beam and they may be bacteriophages but still, we need to have more data to make a comment on whether we detected bacteriophages in these experiments and their mass and stiffness values.

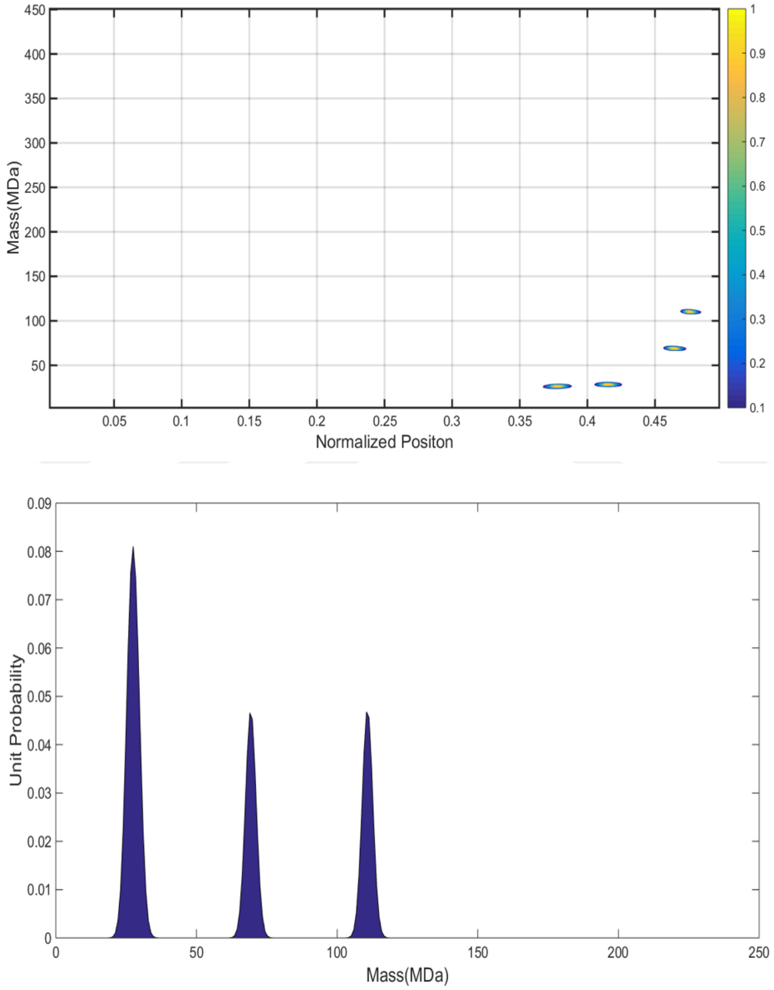

Figure 4.12: (a)Real-time eigenfrequency jumps in first four mechanical modes of doubly clamped beam due to centrosomes.(b) Joint Probability Distribution of mass and position of adsorption of centrosomes (c)The mass distribution of centrosomes

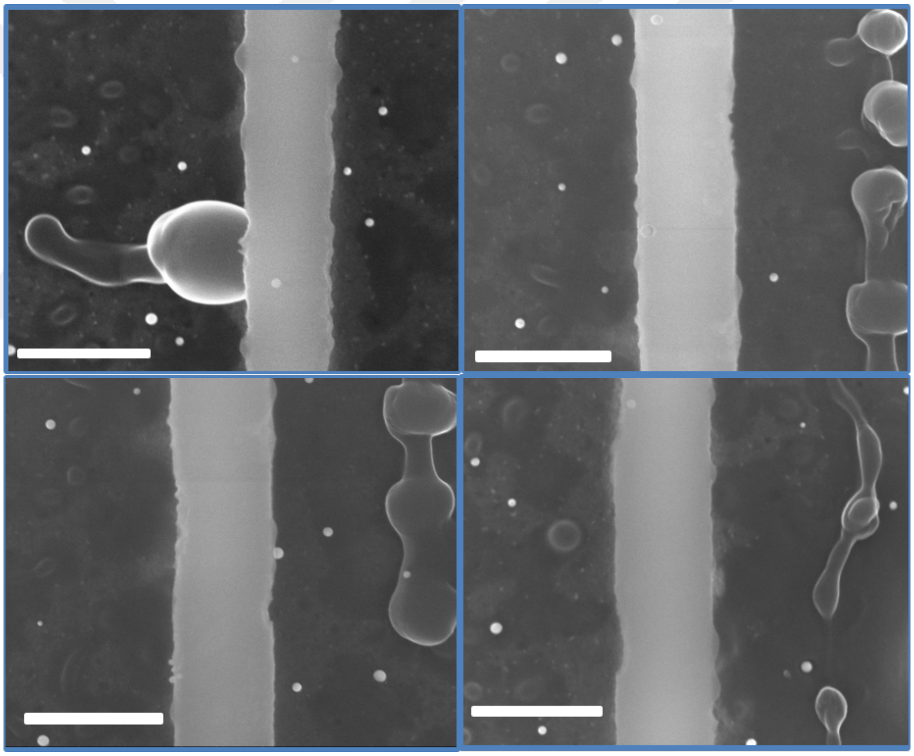

Figure 4.13: SEM Images after Bacteriophages Experiments

Chapter 5

Conclusion and Future Prospect

NEMS has been used in various applications since its first fabrication due its extreme sensitivity and measurement devices respond so fast that it is possible to detect the frequency shifts caused by adsorptions.Thus, they have been used in mass sensing applications for more than a decade. In this M.S. thesis, we fabricated NEMS resonators by collaborating with Sabanci University and utilized those in mass and stiffness spectrometry of nanoparticles and bio-molecules and after coming up with a mathematical model with an assumption of analytes are hemispherical, we presented our results.

NEMS resonators used in this work are in the shape of a doubly clamped beam and its actuation and detection methods are completely electronical. Their transduction covers electrothermal actuation and piezoresistive detection with down-mixing.Electrotermal drive provided capability of multimode actuation, we were able to drive the resonator in four out of plane modes simultaneously. In fabrication of these devices we deployed e-beam lithography for writing the structures, thermal and e- beam evaporation for metallization and dry etch steps to suspend the doubly clamped beam. Scanning Electron and Optical Microscopy were frequently used before and after the experiments.

NEMS-MS requires a delivery mechanism of analytes. Both ESI and MALDI methods which are mostly used in literature so far were tried in this work. First of all, ESI was used to deliver gold nanoparticles and NEMS sensor was kept in low vacuum conditions. Although it was planned that NEMS sensor will be fabricated with KOH backetch in order to create a flow towards the sensor, first experiments were conducted with a suspended NEMS. NEMS was driven in two displacement modes by tracking the frequencies with PLL. In the experiments we could not detect any nanoparticle though. The possible reasons might be that we could not achieve ESI or could not deliver particles towards the sensor.We decided to fabricate sensor with applying KOH back etch and saw that it is a tough and tedious to fabricate these resonators.

MALDI was another method that we tried and gold nanoparticles, centrosomes from HeLa cells and Mke13 bacteriophages were used as analytes in NEMS-MS experiments. While GNPs act as both matrix and analyte, bio-molecules requires matrix addition that absorb laser energy. Ionic Liquid Matrix (ILM) salt was chosen for this purpose. Experiments were conducted in UHV capable chamber and NEMS pcb was placed on the cryostat. First set of GNP data were obtained in cyrogenic temperatures and NEMS device was driven in four out of plane modes and PLL kept the device in resonance conditions during particle adsorption. Measurement in low temperatures reduces frequency instability and promote physisorption. After we realized that there was not an order of magnitude difference between cryogenic and room temperature experiments and we still could detect events, we decided to continue in room temperatures. The data of bio-molecules was very infrequent in comparison to GNPs and their position information was not various along the beam. Thus, we concluded that there might be uniform deposition rather than a single molecule adsorption among data set. Thus, MALDI is not a good alternative for bio-molecules.

Finally, we improved the recently developed theoretical model by assuming that the adhered particles are hemispherical rather than a prismatic or rod-like shape in order to get stiffness and mass of analytes. This assumption was evaluated as a better approximation since we do not know the orientation of bio-molecules on the beam.

These results prove that NEMS is capable of single molecule mass and stiffness spectrometry.The bio-molecule experiments in this study can be improved further in future. We had started to construct a new set-up for ESI, bio-molecule experiments can be done with ESI instead of MALDI. If there is a uniform deposition resulted from matrix material as stated in chapter 4, ESI may overcome this problem.

One of the goals of multimode measurements was to be able to get the size information. Although our theoretical calculations includes this size effect, we can not decouple size and density yet. Using higher order mechanical modes can solve this problem. Thus, even if we do not know anything about the material of the analytes, we can obtain the density, size, stiffness and position values of them.

Bibliography

[1] X. Huang, X. Feng, C. Zorman, M. Mehregany, and M. Roukes, "Vhf, uhf and microwave frequency nanomechanical resonators," *New Journal of Physics*, vol. 7, no. 1, p. 247, 2005.

[2] Y. T. Yang, C. Callegari, X. L. Feng, K. L. Ekinci, and M. L. Roukes, "Zeptogram-scale nanomechanical mass sensing," *Nano Letters*, vol. 6, no. 4, pp. 583–586, 2006.

[3] J. Tamayo, P. M. Kosaka, J. J. Ruz, Á. San Paulo, and M. Calleja, "Biosensors based on nanomechanical systems," *Chemical Society Reviews*, vol. 42, no. 3, pp. 1287–1311, 2013.

[4] M. Li, H. X. Tang, and M. L. Roukes, "Ultra-sensitive nems-based cantilevers for sensing, scanned probe and very high-frequency applications," *Nature nanotechnology*, vol. 2, no. 2, p. 114, 2007.

[5] I. Bargatin, E. Myers, J. Aldridge, C. Marcoux, P. Brianceau, L. Duraffourg, E. Colinet, S. Hentz, P. Andreucci, and M. Roukes, "Large-scale integration of nanoelectromechanical systems for gas sensing applications," *Nano letters*, vol. 12, no. 3, pp. 1269–1274, 2012.

[6] E. Sage, A. Brenac, T. Alava, R. Morel, C. Dupré, M. S. Hanay, M. L. Roukes, L. Duraffourg, C. Masselon, and S. Hentz, "Neutral particle mass spectrometry with nanomechanical systems," *Nature communications*, vol. 6, p. 6482, 2015.

[7] G. Chen, T. Thundat, E. Wachter, and R. Warmack, "Adsorption-induced

surface stress and its effects on resonance frequency of microcantilevers," *Journal of Applied Physics*, vol. 77, no. 8, pp. 3618–3622, 1995.

[8] N. V. Lavrik and P. G. Datskos, "Femtogram mass detection using photothermally actuated nanomechanical resonators," *Applied Physics Letters*, vol. 82, no. 16, pp. 2697–2699, 2003.

[9] K. L. Ekinci, X. M. H. Huang, and M. L. Roukes, "Ultrasensitive nanoelectromechanical mass detection," *Applied Physics Letters*, vol. 84, no. 22, pp. 4469–4471, 2004.

[10] S. Dohn, R. Sandberg, W. Svendsen, and A. Boisen, "Enhanced functionality of cantilever based mass sensors using higher modes," *Applied Physics Letters*, vol. 86, no. 23, p. 233501, 2005.

[11] S. Dohn, W. Svendsen, A. Boisen, and O. Hansen, "Mass and position determination of attached particles on cantilever based mass sensors," *Review of Scientific Instruments*, vol. 78, no. 10, 2007.

[12] S. Schmid, S. Dohn, and A. Boisen, "Real-time particle mass spectrometry based on resonant micro strings.," *Sensors (Basel, Switzerland)*, vol. 10, no. 9, pp. 8092–8100, 2010.

[13] B. Lassagne, D. Garcia-Sanchez, A. Aguasca, and A. Bachtold, "Ultrasensitive mass sensing with a nanotube electromechanical resonator," *Nano letters*, vol. 8, no. 11, pp. 3735–3738, 2008.

[14] H.-Y. Chiu, P. Hung, H. W. C. Postma, and M. Bockrath, "Atomic-scale mass sensing using carbon nanotube resonators," *Nano letters*, vol. 8, no. 12, pp. 4342–4346, 2008.

[15] J. Chaste, A. Eichler, J. Moser, G. Ceballos, R. Rurali, and A. Bachtold, "A nanomechanical mass sensor with yoctogram resolution," *Nature nanotechnology*, vol. 7, no. 5, p. 301, 2012.

[16] A. Naik, M. Hanay, W. Hiebert, X. Feng, and M. Roukes, "Towards single-molecule nanomechanical mass spectrometry," *Nature nanotechnology*, vol. 4, no. 7, p. 445, 2009.

[17] M. S. Hanay, S. Kelber, A. Naik, D. Chi, S. Hentz, E. Bullard, E. Colinet, L. Duraffourg, and M. Roukes, “Single-protein nanomechanical mass spectrometry in real time,” *Nature nanotechnology*, vol. 7, no. 9, p. 602, 2012.

[18] J. Ruz, J. Tamayo, V. Pini, P. Kosaka, and M. Calleja, “Physics of nanomechanical spectrometry of viruses,” *Scientific reports*, vol. 4, p. 6051, 2014.

[19] O. Malvar, J. J. Ruz, P. M. Kosaka, C. M. Domínguez, E. Gil-Santos, M. Calleja, and J. Tamayo, “Mass and stiffness spectrometry of nanoparticles and whole intact bacteria by multimode nanomechanical resonators,” *Nature Communications*, vol. 7, p. 13452, 2016.

[20] M. S. Hanay, S. I. Kelber, C. D. O’Connell, P. Mulvaney, J. E. Sader, and M. L. Roukes, “Inertial imaging with nanomechanical systems,” *Nature Nanotechnology*, vol. 10, no. 4, pp. 339–344, 2015.

[21] J. B. Fenn, “Electrospray wings for molecular elephants (nobel lecture),” *Angewandte chemie international edition*, vol. 42, no. 33, pp. 3871–3894, 2003.

[22] K. Tanaka, “The origin of macromolecule ionization by laser irradiation (nobel lecture),” *Angewandte chemie international edition*, vol. 42, no. 33, pp. 3860–3870, 2003.

[23] R. B. Cole, *Electrospray and MALDI mass spectrometry: fundamentals, instrumentation, practicalities, and biological applications.* John Wiley & Sons, 2011.

[24] J. Kool and W. M. Niessen, *Analyzing biomolecular interactions by mass spectrometry.* John Wiley & Sons, 2015.

[25] J. B. Fenn, M. Mann, C. K. Meng, S. F. Wong, and C. M. Whitehouse, “Electrospray ionization for mass spectrometry of large biomolecules,” *Science*, vol. 246, no. 4926, pp. 64–71, 1989.

[26] J. Tamayo, D. Ramos, J. Mertens, and M. Calleja, “Effect of the adsorbate stiffness on the resonance response of microcantilever sensors,” *Applied physics letters*, vol. 89, no. 22, p. 224104, 2006.

[27] K. Ekinci and M. Roukes, "Nanoelectromechanical systems," *Review of scientific instruments*, vol. 76, no. 6, p. 061101, 2005.

[28] I. Bargatin, I. Kozinsky, and M. L. Roukes, "Efficient electrothermal actuation of multiple modes of high-frequency nanoelectromechanical resonators," *Applied Physics Letters*, vol. 90, no. 9, pp. 1–3, 2007.

[29] T. Kouh, M. S. Hanay, and K. L. Ekinci, "Nanomechanical motion transducers for miniaturized mechanical systems," *Micromachines*, vol. 8, no. 4, pp. 1–27, 2017.

[30] M. Sansa, M. Fernández-Regúlez, J. Llobet, Á. San Paulo, and F. Pérez-Murano, "High-sensitivity linear piezoresistive transduction for nanomechanical beam resonators," *Nature Communications*, vol. 5, 2014.

[31] I. Bargatin, E. B. Myers, J. Arlett, B. Gudlewski, and M. L. Roukes, "Sensitive detection of nanomechanical motion using piezoresistive signal downmixing," *Applied Physics Letters*, vol. 86, no. 13, pp. 1–3, 2005.

[32] S. Kelber, "Single-Particle Mass Spectrometry and Inertial Imaging with Nanomechanical Systems Thesis by," 2013.

[33] T. E. Angel, U. K. Aryal, S. M. Hengel, E. S. Baker, R. T. Kelly, E. W. Robinson, and R. D. Smith, "Mass spectrometry-based proteomics: existing capabilities and future directions," *Chemical Society Reviews*, vol. 41, no. 10, pp. 3912–3928, 2012.

[34] S. Schmid, M. Kurek, J. Q. Adolphsen, and A. Boisen, "Real-time single airborne nanoparticle detection with nanomechanical resonant filter-fiber," *Scientific Reports*, vol. 3, pp. 3–7, 2013.

[35] M. J. Madou, *Manufacturing techniques for microfabrication and nanotechnology*, vol. 2. CRC press, 2011.

[36] J. E. Sader, M. S. Hanay, A. P. Neumann, and M. L. Roukes, "Mass spectrometry using nanomechanical systems: beyond the point-mass approximation," *Nano letters*, vol. 18, no. 3, pp. 1608–1614, 2018.

[37] J. A. Crank and D. W. Armstrong, “Towards a second generation of ionic liquid matrices (ilms) for maldi-ms of peptides, proteins, and carbohydrates,” *Journal of the American Society for Mass Spectrometry*, vol. 20, no. 10, pp. 1790–1800, 2009.

[38] N. Stephen, “On energy harvesting from ambient vibration,” *Journal of sound and vibration*, vol. 293, no. 1-2, pp. 409–425, 2006.

[39] M. T. Spencer, H. Furutani, S. J. Oldenburg, T. K. Darlington, and K. A. Prather, “Gold nanoparticles as a matrix for visible-wavelength single-particle matrix-assisted laser desorption/ionization mass spectrometry of small biomolecules,” *The Journal of Physical Chemistry C*, vol. 112, no. 11, pp. 4083–4090, 2008.

[40] D. W. Armstrong, L.-K. Zhang, L. He, and M. L. Gross, “Ionic liquids as matrixes for matrix-assisted laser desorption/ionization mass spectrometry,” *Analytical chemistry*, vol. 73, no. 15, pp. 3679–3686, 2001.

Appendix A

Code

A.1 Calculation According to Hemisphere Approximation

```
clear
%% Mode Shapes From Comsol
filename = strcat('mode_shapes_new.txt');
[x1,u1]= textread(filename,'%f %f','headerlines',8);
% Normalization of first 4 modes
    for k=1:6
    i= length(x1)/6;
    modes{k}=u1(1+(k-1)*i:i*k);
    modes{k}=modes{k}./sqrt(sum(modes{k}.^2)/length(modes{k}));
    end
phi1 = modes{1}; phi2=modes{2}; phi3=modes{4}; phi4=-1*modes{6};
%% Get experimental fractional frequency shifts

load('data_allcentrosome_1_2_4.mat');
events = length(data);
```

```
%data(12,:)=[];
 for event = 1:length(data);
 fjumps_exp = data(event,1:4);
  x_a_exp = data(event,5);
%  r_a_exp = data(event,7)/2;

%% Useful Parameters
 L_b   = 15e-6;  %m
 rho_b = 3300;   %kg/m^3
 w_b   = 370e-9; %m
 t_b   = 100e-9; %m
 M_b   = L_b*t_b*w_b*rho_b;  %kg
 E_b   = 241e9; %Pa
%M_b   = L_b*t_b*w_b*rho_b;  %kg
%M_b = 1.8126e-15;

% Useful Terms
% Calculate psi = d^2phi(x)/dx^2
 psi1 = diff(phi1,2)*(length(phi1)-1)^2/L_b^2;
 psi2 = diff(phi2,2)*(length(phi2)-1)^2/L_b^2;
%psi3 = diff(phi3,2)*(length(phi3)-1)^2/L_b^2;
 psi4 = diff(phi4,2)*(length(phi4)-1)^2/L_b^2;
%Integral
n = length(psi1);
x = linspace(0,1,n);
%Calculate integral(d^2phi(x)/dx^2)
c1= trapz(x,psi1.^2)*L_b;    c2= trapz(x,psi2.^2)*L_b;
%c3= trapz(x,psi3.^2)*L_b;
c4= trapz(x,psi4.^2)*L_b;
%Calculate dphi(x)/dx
g1 = diff(phi1)*(length(phi1)-1)/L_b;
g2 = diff(phi2)*(length(phi2)-1)/L_b;
%g3 = diff(phi3)*(length(phi3)-1)/L_b;
```

```
g4 = diff(phi4)*(length(phi4)-1)/L_b;

%% Solving a system of Nonlinear Equations
x_a_exp = data(event,5);
x_a_try = x_a_exp-0.05:0.001:x_a_exp+0.05;
rho_a_try =1300;

min_err = inf;
for i = 1:length(x_a_try)
  for j = 1:length(rho_a_try)

   x_a = x_a_try(i);
   rho_a = rho_a_try(j);
%  index = find(abs((x-x_a)) < 5e-4);
%  if length(index)>1
%     index = index(1);
%  end
    [~,index] = min(abs(x-x_a));
    alpha1 = -6*psi1(index)^2/c1;
    alpha2 = -6*psi2(index)^2/c2;
    %alpha3 = -6*psi3(index)^2/c3;
    alpha4 = -6*psi4(index)^2/c4;

    beta1 = 1/3*phi1(index)^2;
    beta2 = 1/3*phi2(index)^2;
    %beta3 = 1/3*phi3(index)^2;
    beta4 = 1/3*phi4(index)^2;

    %Least Square Method by using 4 fjumps together
A = [alpha1 beta1;alpha2 beta2;alpha4 beta4];
b = fjumps_exp([1 2 4])'*1e-4;
u = inv(A'*A)*A'*b;
```

```
%%Perfect match for the first 2 fjumps errors will be in the
%fjumps3 and 4
%  A = [alpha1 beta1;alpha2 beta2;alpha4 beta4];
%  b = fjumps_exp([1 2 4])'*1e-4;
%  u = A\b;

r = (u(2)*M_b/rho_a/pi)^(1/3);
V_a = 2/3*pi*r^3;
E_a = u(1)*(E_b*t_b*w_b/(V_a*(1/4+r/t_b*3/8+r^2/t_b^2*1/5)));

F1 = -1/2*(E_a*(psi1(index)^2*2/3*pi)/...
(E_b*w_b*t_b/12*c1)*(r^3/4+r^4/t_b*3/8+r^5/t_b^2*1/5)...
-2/3*pi/M_b*rho_a*(phi1(index)^2*r^3+(g1(index)^2 ...
+phi1(index)*psi1(index))*r^5/5));

F2 = -1/2*(E_a*(psi2(index)^2*2/3*pi)/...
(E_b*w_b*t_b/12*c2)*(r^3/4+r^4/t_b*3/8+r^5/t_b^2*1/5)...
-2/3*pi/M_b*rho_a*(phi2(index)^2*r^3+(g2(index)^2 ...
+phi2(index)*psi2(index))*r^5/5));

%F3 = -1/2*(E_a*(psi3(index)^2*2/3*pi)/...
%(E_b*w_b*t_b/12*c3)*(r^3/4+r^4/t_b*3/8+r^5/t_b^2*1/5)...
% -2/3*pi/M_b*rho_a*(phi3(index)^2*r^3+(g3(index)^2 ...
%+phi3(index)*psi3(index))*r^5/5));

F4 = -1/2*(E_a*(psi4(index)^2*2/3*pi)/ ...
(E_b*w_b*t_b/12*c4)*(r^3/4+r^4/t_b*3/8+r^5/t_b^2*1/5)...
-2/3*pi/M_b*rho_a*(phi4(index)^2*r^3+(g4(index)^2+ ...
 phi4(index)*psi4(index))*r^5/5));

fjumps_try = [F1 F2 F4]*1e4;
Allan=[2e-6 2e-6 2e-6 2e -6];
fjumps_exp;
```

```
%error = sqrt(mean((abs(fjumps_exp(1:3)- ...
%fjumps_try(1:3))./fjumps_exp(1:3).*...
 %([fjumps_exp(1) fjumps_exp(2) fjumps_exp(3) ] ...
%/norm([fjumps_exp(1) fjumps_exp(2) fjumps_exp(3)]))).^2));

 error = (fjumps_exp(1)*1e-4/Allan(1))^2 ...
 *((fjumps_exp(1)-fjumps_try(1))*1e-4)^2 ...
 +(fjumps_exp(2)*1e-4/Allan(2))^2 ...
 *((fjumps_exp(2)-fjumps_try(2))*1e-4)^2 ...
 +(fjumps_exp(4)*1e-4/Allan(3))^2 ...
 *((fjumps_exp(4)-fjumps_try(3))*1e-4)^2;
%error = (fjumps_exp(1)*1e-4-fjumps_try(1)*1e-4)^2/Allan(1)^2+ ...
%(fjumps_exp(2)*1e-4-fjumps_try(2)*1e-4)^2/Allan(2)^2 ...
%+(fjumps_exp(3)*1e-4-fjumps_try(3)*1e-4)^2/Allan(3)^2;

 if (E_a<E_b) && E_a>0 &&(error < min_err)
     min_err=error;
     optimal_quad = [ x_a,r, E_a,rho_a];
     x_a_calculated = optimal_quad(1);
     E_a_calculated = optimal_quad(2);
     r_a_calculated = optimal_quad(3);
     rho_a_calculated = optimal_quad(4);
     mass= 2/3*pi*rho_a*r^3*6.02214086e20 ; %MDa
     table{event} = [x_a_calculated,r_a_calculated, ...
     E_a_calculated, rho_a_calculated,fjumps_try mass];
    end
  end
end
end
```

A.2 Plotting Calculated and Expected Values of Size, Stiffness and Position

```
clc
close all
for i=1:length(data)

    x_a_calculated(i) = table{i}(1);
    E_a_calculated(i) = table{i}(2);
    r_a_calculated(i) = table{i}(3);
    rho_a_calculated(i) = table{i}(4);
    fjumps_calculated((i-1)*4+1:(i-1)*4+4) = table{i}(5:end);

    fjumps_exp((i-1)*4+1:(i-1)*4+4) = data(i,1:4);
    x_a_exp(i) = data(i,5);
    r_a_exp(i) = 15e-9;
    E_a_exp(i) = 80e9;
    rho_a_exp(i) = 19300;
end
error_all=[];
for event = 1:length(data)
 for i=1:4
    err(i) = sqrt(mean(((fjumps_exp(i+4*(event-1))-
    ...fjumps_calculated(i+4*(event-1)))./fjumps_exp(i+4 ...
    *(event-1))).^2))*100;

end
error_place=[];
error1{event}=err(1:4)
x=1:4;
y=ones(1,4)*event;
stem3(y,x,err,'LineWidth',5)
```

```
hold on
end
set(gca,'fontweight','bold','fontsize',20)
xlabel('Number of Modes')
ylabel('Mode Number')
zlabel('%Error')
figure
plot(1:length(data),E_a_calculated*1e-9,'LineWidth',3)
hold on
plot(1:length(data),E_a_exp*1e-9,'LineWidth',3)
xlabel('Number of Events','fontsize',20)
ylabel('Youngs Modulus Estimation(GPa)','fontsize',20)
legend(['Calculated' ], ['Expected'],'Location','NorthWest')
set(gca,'fontweight','bold','fontsize',20)

figure
plot(1:length(data),x_a_calculated ,'LineWidth',3)
hold on
plot(1:length(data),x_a_exp ,'LineWidth',3)
xlabel('Number of Events','fontsize',20)
ylabel('Position Estimation','fontsize',20)
legend(['Calculated' ], ['Experiment'],'Location','NorthWest')
set(gca,'fontweight','bold','fontsize',20)

figure
plot(1:length(data),r_a_calculated*1e9,'LineWidth',3)
hold on
plot(1:length(data),r_a_exp*1e9,'LineWidth',3)
xlabel('Number of Events','fontsize',20)
ylabel('Radius Estimation (nm)','fontsize',20)
legend(['Calculated' ], ['Experiment'],'Location','NorthWest')
set(gca,'fontweight','bold','fontsize',20)
```